

1 **Sandstone-filled normal faults: A case study from central California**

2 Giuseppe Palladino^{a,*}, G. Ian Alsop^{a,*}, Antonio Grippa^a, Gustavo Zvirtes^a, Ruy Paulo
3 Phillip^b, Andrew Hurst^a

4
5 ^aDepartment of Geology and Petroleum Geology, School of Geosciences, University
6 of Aberdeen, Aberdeen, UK

7 ^bDepartamento de Mineralogia e Petrologia, Universidade Federal do Rio Grande do
8 Sul, Porto Alegre, Rio Grande do Sul, Brazil

9 10 **Abstract**

11 Despite the potential of sandstone-filled normal faults to significantly influence
12 fluid transmissivity within reservoirs and the shallow crust, they have to date been
13 largely overlooked. Fluidized sand, forcefully intruded along normal fault zones,
14 markedly enhances the transmissivity of faults and, in general, the connectivity
15 between otherwise unconnected reservoirs. Here, we provide a detailed outcrop
16 description and interpretation of sandstone-filled normal faults from different
17 stratigraphic units in central California. Such faults commonly show limited fault
18 throw, cm to dm wide apertures, poorly-developed fault zones and full or partial sand
19 infill. Based on these features and inferences regarding their origin, we propose a
20 general classification that defines two main types of sandstone-filled normal faults.
21 Type 1 form as a consequence of the hydraulic failure of the host strata above a
22 poorly-consolidated sandstone following a significant, rapid increase of pore fluid
23 over-pressure. Type 2 sandstone-filled normal faults form as a result of regional

24 tectonic deformation. These structures may play a significant role in the connectivity
25 of siliciclastic reservoirs, and may therefore be crucial not just for investigation of
26 basin evolution but also in hydrocarbon exploration.

27

28 **1. Introduction**

29 Understanding the architecture of fault zones has become increasingly
30 important as their characteristics have a significant influence on the migration and
31 entrapment of fluids in the subsurface. In particular, the permeability of fault rocks
32 plays a fundamental role in fluid transmissibility (e.g. Childs et al., 2007). Faults
33 affecting shallow crustal strata commonly display a wide range of fault zone
34 architecture, which varies from very thin gouge or cataclastic horizons, to well-
35 developed damage and core zones (Caine et al., 1996; Kim et al., 2004). In multi-
36 layered, poorly-consolidated, siliciclastic strata (mudstone-sandstone intercalations),
37 fault rocks are typically represented by cataclastic mixtures of sandstone and
38 mudstone smeared along the fault walls. Fine-grained particulate flow, cataclastic
39 material and highly smeared clay content are all factors which hinder fluid flow
40 migration and significantly promote reservoir compartmentalization (Jones et al.
41 1998; Bailey et al., 2002; Bense et al., 2003; Ainsworth, 2006; Childs et al. 1997;
42 2007; Jolley et al. 2007; Fredman et al., 2007). Mineralization, sourced from fluids
43 percolating through a fault zone, is an additional factor that precludes subsequent
44 fluid migration through fault zones. On the other hand, the occurrence of porous and
45 permeable sandstone within a fault zone may strongly enhance its fluid migration
46 capacity.

47 Sand can be incorporated into fault zones due to a variety of reasons listed
48 below (Lewis et al., 2002): i) beds of sandstone are sheared and form deformed
49 ribbons parallel to a fault plane; ii) beds of sandstone are dragged and rotated until
50 they become parallel to the fault plane; iii) fluidized sand is injected along the fault
51 zone discontinuities. Here we focus on the latter case. Two essential preconditions
52 are required for sand fluidization to occur along a fault plane: i) the velocity of flow
53 along the fault plane must be high enough for sand grains to be fluidised; ii) the
54 parent sandstone from which fluidised sand is derived is poorly-consolidated. The
55 first condition is encountered when the velocity of the fluid exceeds the minimum-
56 fluidization velocity of sand (Lowe, 1975). The second condition usually occurs in
57 parts of sedimentary basins that never experienced significant diagenetic
58 modification, and is commonly confined to the first few hundreds of metres of burial
59 (Jonk et al., 2003; Vigorito and Hurst, 2010).

60 Although sandstone intrusions associated with normal faults are occasionally
61 interpreted using subsurface data (Dixon et al., 1995; Shoulders et al., 2007; Koša,
62 2007; Bureau et al. 2013; Yang et al., 2014), they are still poorly-documented at
63 outcrop (Taylor, 1982; Audemard and de Santis, 1991; Jolly and Lonergan, 2002;
64 Lewis et al., 2002; Ribeiro and Terrinha, 2007; Montenat et al., 2007; Siddoway and
65 Gehrels, 2014; Ravier et al., 2015; Palladino et al., 2016; Siddoway et al., 2017). Our
66 case study therefore focuses on well-developed sandstone-filled normal faults
67 (SFNF) exposed in the Panoche/Tumey hills and Santa Cruz areas in central
68 California (Fig. 1), where mainly deep-water clastic strata present ideal conditions for
69 sand intrusion along faults. The aim of this paper is to document these exceptional
70 field examples of SFNF, and to discuss their geometry, origin, timing, and
71 mechanism of emplacement. Their significance in terms of basin evolution, and the

72 potential role they play as either conduits or barriers to fluid flow in hydrocarbon
73 reservoirs is discussed.

74

75 **2. Geological Setting**

76 *2.1. Panoche/Tumey hills area stratigraphy*

77 The Panoche/Tumey hills area comprises a Late Cretaceous to Early
78 Cenozoic stratigraphic sequence deposited along the western margin of the San
79 Joaquin Valley (Moxon, 1988) (Fig. 1a). The San Joaquin Valley infill consists of a
80 thick accumulation of Jurassic to Quaternary marine and non-marine clastic strata
81 that unconformably overlie the Franciscan Complex. Due to its position along an
82 active basin margin, the Panoche-Tumey hills area experienced numerous tectonic
83 phases in different geodynamic contexts. SFNF are found within the Moreno and
84 Kreyenhagen Shale formations both deposited in an ancient forearc basin (Fig. 1a).
85 The Moreno Formation consists of an Upper Cretaceous to Lower Paleocene
86 sequence of lens-shaped turbiditic sandstone, mudstone and diatomaceous
87 mudstone that were deposited in a base-of-slope to the upper slope-shelf
88 environment. The Kreyenhagen Shale (Eocene) comprises a dominantly mudstone
89 sequence containing isolated turbiditic sandstone deposited in a slope to shelf
90 environment (Moxon, 1988; Bartow, 1991; Johnson and Graham, 2007). The upper
91 part of this formation consists of thick packages of diatomaceous mudstones.

92

93 *2.2. Santa Cruz area stratigraphy*

94 The Santa Cruz coastal area consists of a Miocene sedimentary succession
95 that unconformably overlies the granitic/metamorphic Salinian basement (Clark,
96 1981; Aydin and Page, 1984; Page et al., 1998) (Fig. 1b). This sedimentary
97 succession consists of the coarse-grained, large-scale cross-bedded tidal/nearshore
98 arkosic Santa Margarita Sandstone, which passes upward into deep-water to shelfal,
99 organic-rich, thickly bedded biosiliceous Santa Cruz Mudstone (Fig. 1b) (Barron,
100 1986). The Miocene to Pliocene Purisima Formation is the youngest unit recognized
101 in the Santa Cruz area, and comprises, very thick-bedded tuffaceous and
102 diatomaceous neritic siltstones alternating with thick-bedded andesitic sandstones
103 (Johnson and Graham, 2007).

104

105 *2.3. Tectonic setting*

106 The present structural arrangement of central California (including the two
107 study areas) (Fig. 1), is mainly the result of contractional and strike-slip tectonics
108 operating from the Cretaceous to the Quaternary (Page et al., 1998; Atwater and
109 Stock, 1998). Contractional tectonics resulted from the accretion of the Franciscan
110 complex and the concomitant onset of the Great Valley forearc basin (Ingersoll,
111 1979; Dickinson and Seely, 1979; Constenius et al., 2000). Strike-slip tectonics is
112 related to the activation of the San Andres Fault zone and other associated faults
113 from the Eocene onward (Sharman et al., 2013). The Panoche/Tumey hills area is
114 located along the eastern flank of the San Joaquin Valley which is part of the Great
115 Valley Basin. Its structure consists of a series of anticlines and synclines often
116 marked at base by thrust planes (Bartow, 1991; Namson and Davis, 1988). The
117 Santa Cruz area consists of a southwest-dipping homocline situated between the

118 San Andreas Fault Zone (SAFZ) and San Gregorio Fault Zone (SGFZ) (see Fig. 1
119 map inset) (Phillips, 1990).

120 Despite the lack of extensional tectonics in this regional tectonic context, the
121 number of normal faults in the study areas is surprisingly high and many of these
122 structures are actually SFNF. The origin of these normal faults is poorly addressed in
123 the literature, although normal fault orientation is often consistent with either outer
124 arc extension in contractional structures (e.g. Palladino et al, 2016) or associated
125 with wrench tectonics (Aydin and Page, 1984). Another possibility for the initiation of
126 normal faults is linked to the exhumation of the Franciscan complex, which is
127 accommodated by extensional tectonics (Krueger and Jones, 1989; Dumitru, 1989;
128 Harms et al., 1992; Unruh et al., 2007; Sousa et al., 2016). In the Panoche/Tumey
129 hills area, the majority of SFNF are systematically oriented NW-SE and WNW-ESE
130 (Fig. 2a), whereas in the Santa Cruz coastal area, the normal faults are dominantly
131 NNW-SSE and N-S trending (Fig. 2b).

132 Although accurate time constraints for SFNF are difficult to ascertain, field
133 observations do provide some important constraints. For example, in the
134 Panoche/Tumey hills area (Fig. 2), SFNF are not documented in stratigraphic units
135 younger than the Kreyenhagen Shale and abruptly terminate at the unconformity
136 delimiting the base the Temblor Formation. This allows us to constrain the age of
137 tectonic deformation to between the middle Eocene (age of the Kreyenhagen Shale)
138 and the Middle Miocene (age of the Temblor Formation). In the Santa Cruz area
139 (Fig. 2), the timing of faulting is less well constrained. As the age of the Santa Cruz
140 Mudstone, the stratigraphic unit hosting SFNF, has been attributed to 7-9 Ma (Late
141 Miocene) (Boehm and Moore 2002), the age of the normal faulting is younger than

142 this. However, the lack of younger units covering SFNF in this area does not allow us
143 to bracket the youngest possible age.

144

145 *2.4. Sand injection complexes in central California*

146 At least three significant sand injection complexes are recognized in central
147 California (Fig. 1): the Panoche Giant Injection complex (PGIC), the Tumey Giant
148 Injection Complex (TGIC) and, the significantly smaller-scale Santa Cruz Injection
149 Complex (SCIC), which comprises several periods of sand injection including sand
150 extrusion (Thompson et al., 1999; Scott et al., 2009; Vigorito et al., 2008; Hurst et al.,
151 2011).

152

153 *2.4.1. Panoche Giant Injection complex (PGIC)*

154 The PGIC (Fig. 1a) consists of a well-defined network of dikes and sills
155 intruded within the Upper Cretaceous to Paleocene Moreno Formation (Vigorito and
156 Hurst, 2010). This injection complex records a large-scale overpressure event that
157 occurred during the Lower Paleocene (Danian) and involved an area of at least 1500
158 km² that includes almost 400 km² of outcrop (Vigorito and Hurst, 2010). It consists of
159 different architectural elements represented (from the base to top) by parent units,
160 intrusive bodies and extrudites (Vigorito et al., 2008; Hurst et al., 2011; Scott et al.,
161 2013). PGIC parent units comprise turbiditic channel-complexes and isolated
162 sandstone channels occurring in the lower portion of the Moreno Formation (Vigorito
163 et al., 2008). The intrusive bodies consist of cm- to metre- thick interconnected single
164 or multi-layered sills and dikes. Extrudites (Vigorito and Hurst, 2010) comprise

165 mound-like sand bodies cropping out in the Upper part of the Moreno Formation,
166 where they consist of fine- to medium-grained sands linked to the underlying
167 intrusive complex by isolated dikes.

168

169 *2.4.2. Tumey Giant Injection Complex (TGIC)*

170 The TGIC (Fig. 1a) consists of a network of dikes and sills emplaced in the
171 Kreyenhagen Shales (Huuse et al., 2007). The TGIC differs from the PGIC in that it
172 has extensive channelized turbiditic sandstones that are intensely deformed by sand
173 fluidization throughout the injection complex. Sand extrudites are absent in the TGIC,
174 which if ever present were removed by later erosion. The absence of extrudites
175 precludes bracketing the precise timing of sand injection. However, the TGIC
176 intrudes the Kreyenhagen Shale strata of lower to middle Eocene age, and the
177 timing of sand injection cannot be older than this. The Miocene Temblor Formation
178 which unconformably overlies the Kreyenhagen Shale is unaffected by sand
179 injection, meaning that injection pre-dates this unit.

180

181 *2.4.3. Santa Cruz Injection Complex (SCIC)*

182 The SCIC (Fig. 1b) consists of a network of partially tar-saturated and
183 unsaturated dikes and sills emplaced in the Santa Cruz Mudstone (Thompson et al.,
184 1999; Scott et al. 2009). The parent unit of the SCIC is commonly identified as the
185 Santa Margarita Sandstone (Boehm and Moore, 2002; Thompson et al., 2007).
186 Using mineralogical data Clark (1981) and Scott et al. (2009) suggested that multiple
187 parent sandstones existed. The injection complex has a well-developed intrusive

188 network that mainly consists of widely-spaced sills, dikes and locally preserved
189 saucer-shaped intrusions. Individual intrusions generally have thicknesses which
190 range from a few centimetres to a decimetre. Isolated dikes or sills are up to a few
191 metres wide with the Yellowbank/Panther beach sill at least up to 15 m thick
192 (Thompson et al., 1999; Scott et al., 2009). Extruded sands occur as multiple,
193 laterally-discontinuous, mounded units recognized in different stratigraphic levels in
194 the Santa Cruz Mudstone (Boehm and Moore 2002; Hurst et al. 2006). The
195 occurrence of extrudites within the Santa Cruz Mudstone allows the age of
196 emplacement of the SCIC to be constrained to the Late Miocene (7–9 Ma).

197

198 **3. Characteristics of normal faults hosting sand injections in central California**

199 The majority of normal faults recognized in the Panoche/Tumey hills and
200 Santa Cruz areas display a range of similarities including: i) moderate to steeply
201 dipping planar to gently undulating fault surfaces, ii) cm to m-scale offsets and iii)
202 graben-like geometry. However, some significant differences linked to the lithology
203 and physical state of the strata at the time of deformation also exist, and these
204 strongly influence the characteristics of the fault zone. Therefore, in order to better
205 understand the mechanical behaviour of SFNF, it is first necessary to describe the
206 main characteristics of the stratigraphic successions cut by these faults.

207 In the Panoche/Tumey hills area (Fig. 1a), faulted successions consist of
208 poorly-consolidated sandstone alternating with packages of mudstone (Fig. 3a, b).
209 The units of interest are the Moreno and the Kreyenhagen Shale formations which
210 are characterized by significant physical anisotropy, with high permeability measured
211 parallel to the bedding planes, and low permeability measured orthogonal to this

212 (Bense and Person, 2006). Hereafter this is referred to as the Panoche/Tumey-type
213 successions.

214 In the Santa Cruz coastal area (Fig. 1b), the faulted succession predominantly
215 consists of well-consolidated bio-siliceous mudstone belonging to the Santa Cruz
216 Mudstone (Fig. 3c, d). Excluding the rare occurrence of a faint parallel lamination,
217 occasional claystone horizons and isolated sandstone bodies, these bio-siliceous
218 mudstones can be considered as an isotropic succession with low permeability in all
219 directions. In this case, the permeability is essentially linked to the secondary
220 porosity created by fracture networks developed in close proximity to tectonic
221 disturbance zones. Hereafter this is referred to as the Santa Cruz-type succession.

222 When different types of lithology such as the Panoche/Tumey- and Santa
223 Cruz-type successions are involved in deformation, the resulting fault rocks and fault
224 zones show significant variability. Fault zones mainly consist of three elements
225 represented by the fault core, damage zone, and undeformed protolith (Caine et al.,
226 1996; Braathen et al., 2009). The fault core is the portion of the fault zone where
227 most of the displacement is accommodated. In the shallow crust, at a depth of less
228 than 1 km, fault cores commonly consist of gouge, breccia, cataclasite/particulate
229 flow and smeared clay. This portion generally forms a low permeability zone within
230 the fault (Knipe et al., 1998; Bense et al., 2003; Bense and van Balen, 2003; Ballas
231 et al., 2015; Peacock et al., 2017). The damage zone forms the intermediate region
232 between the fault core and the undisturbed protolith, and is characterized by small
233 faults and fractures, that are distinguished either by high or low permeability,
234 depending on the lithological characteristics of the protolith. As the fault core can be
235 discontinuously distributed along the fault zone, so that it does not necessarily form a
236 continuous barrier, the fundamental element controlling fluid transmission and,

237 consequently, the emplacement of sand along the fault plane, is the damage zone
238 itself. Depending on fault rock consolidation, the damage zone can display open or
239 closed fractures, while the width of the damage zone is generally observed to
240 increase with larger fault throws (e.g., Knott et al., 1996; Manzocchi et al., 1999;
241 Childs et al., 2009).

242 Damage zones developed in Panoche/Tumey-type successions are generally
243 characterized by closed-fracture networks, cataclastic/deformation bands and mixing
244 zones where sand/mud mixing processes contribute to further reduce the
245 permeability (Heynekamp et al., 1999; Rawling et al., 2001; Bense et al., 2003;
246 Loveless et al., 2011) (Fig. 3b). The average fault zone width ranges from millimetres
247 to some tens of decimetres. Also, the width of the core zone is sometimes dominant
248 with respect to the damage zone thickness. In addition, the width of a fault zone
249 developed in mudstone/sandstone alternations can vary parallel to the fault plane,
250 resulting in the more sandstone-rich parts of the fault zone being wider than those
251 that are dominated by mudstone (Sperrevik et al., 2002; Bense and Person, 2006).

252 In Santa Cruz-type successions damage zones produce a very different
253 permeable, dense, open-fracture network that surrounds the fault core (Fig. 3d).
254 Based on field observations, the fracture network width is directly proportional to the
255 fault throw. It can often extend laterally for many metres or tens of metres so that,
256 the width of the core zone, which can range from some decimetres to 1m, is
257 negligible when compared with the width of the entire fault zone.

258 Low and high permeability damage zones therefore form two end-members
259 that are observed in the Santa Cruz coastal sector and in the Panoche/Tumey hills
260 area respectively. They reflect the brittle and ductile behaviour of the strata involved

261 in the deformation. The differences observed in the two fault zones end-members
262 have a marked impact on conditioning the fluid flow and, consequently, the spatial
263 distribution and geometry of the sandstone intrusions associated with the SFNF.

264

265 **4. SFNF classification**

266 Based on our field observations, it is possible to distinguish two main types of
267 SFNF (Fig. 4).

268

269 *4.1. Type 1 SFNF*

270 Type 1 SFNF are related to the fluidization of a sandstone parent unit that
271 consists either of pristine depositional sandstones or poorly-lithified sandstone
272 intrusions, and the consequent collapse of the overburden due to the evacuation of
273 sand during an overpressure event (Fig. 4a). The distinctive characteristic of Type 1
274 SFNF is that they nucleate at the top of the remobilized parent unit, and propagate
275 upward without ever cutting through the entire parent sand body. Other important
276 features are the limited vertical extent of these structures, the restricted amount of
277 offset which can vary from a few cm to some metres, and the lack of a well-
278 developed fault zone and associated fault breccias. In most cases, the faults
279 dissipate quickly and resemble syn-depositional faults (Fig. 4a). Evidence for the
280 direction of fluidized sand transport is provided by dragging of layers of the host
281 strata in the sense of the fluid movement, and by the distribution of mudstone clasts
282 along the fault. This suggests that the sand is commonly injected upward, or along-
283 strike. Type 1 SFNF are commonly developed in sill zones (*sensu* Vigorito and
284 Hurst, 2010). Subsurface examples of similar faults have been interpreted previously
285 from the North Sea (Dixon et al., 1995).

286

287 4.2. *Type 2 SFNF*

288 Type 2 SFNF are tectonically-related sandstone-filled normal faults (Fig. 4b).
289 Unlike the previously described Type 1, Type 2 SFNF cut through the entire parent
290 sandstone body. In the study areas, it is possible to distinguish two main sub-
291 categories (Type 2a and Type 2b) that are described below.

292

293 4.2.1. *Type 2a SFNF*

294 Type 2a SFNF are related to episodes of regional extensional tectonics (Fig.
295 4b). They generally consist of a master fault plane and a series of associated
296 antithetic and synthetic minor faults that have small offsets and graben-like
297 geometry. Unlike Type 1 SFNF, Type 2a SFNF do not display a progressive
298 decrease in offset toward terminations. The measured offsets range from a few
299 centimetres to some metres, while apertures can locally reach 1.5 m. The
300 occurrence of dip-slip oriented slickensides provides a clear indication of normal fault
301 kinematics. Fault zones can be variably developed depending on characteristics of
302 the succession, and the injected sand either entirely fills spaces between breccia
303 clasts, or is predominant and contains isolated 'floating' clasts.

304

305 4.2.2. *Type 2b SFNF*

306 SFNF linked to regional contractional tectonics occur as a consequence of
307 outer-arc extension and flexural slip (Fig. 4c). Outer-arc extension produces a series
308 of normal faults that are typically arranged in a radial pattern around fold hinges.
309 They are very common in the Panoche/Tumey hills area (Fig. 1) and are recognized

310 in the field on the basis of their trend, which is commonly subparallel to that of major
311 fold hinges, and by the triangular-shaped geometries that progressively taper
312 downward toward fold cores (Palladino et al., 2016). Small-scale Type 2b SFNF may
313 also develop in association with flexural slip folding of a multi-layered succession.
314 According to Gross et al. (1997), these structures usually form because of pull-apart
315 opening and block rotation mechanisms that create space for syn-tectonic sand
316 injection.

317

318 **5. Outcrop examples of SFNF**

319 SFNF crop out in numerous localities throughout in the Panoche/Tumey hills
320 and Santa Cruz areas. Three key localities, displaying the best preserved SFNF, are
321 selected as outcrop examples and include Tumey Gulch and Monocline Ridge in the
322 Panoche/Tumey hills area, and Panther Beach near Santa Cruz (Fig. 1).

323

324 *5.1. Tumey Gulch*

325 Tumey Gulch, in the southwestern side of the study area, consists of a
326 kilometre-scale anticline in which the Moreno Formation is exposed in the eroded
327 fold core (Fig. 1a). Here, on both flanks of the fold, well-preserved sets of conjugate,
328 closely-spaced, Type 1 and Type 2 SFNF are preserved. Two outcrops, named O1
329 and O2, are considered below.

330 Type 1 SFNF recognized in the outcrop O1 consists of conjugate normal
331 faults that display small (cm) offsets and sandstone-filled apertures of a few
332 centimetres (Fig. 5a). Faults die out upward over tens of centimetres, so that the

333 overlying beds remain unaffected by deformation (Fig. 5b, c). These SFNF are
334 located in the lower portion of the Moreno Formation and, in particular, at the top of
335 strongly remobilized sandstone units belonging to the PGIC.

336 The outcrop O2 shows both Type 1 and Type 2b SFNF. In Fig. 6 an array of
337 Type 1 SFNF overlies a deformed, lens-shaped turbidite channel sandstone, which
338 is at least 2 m thick and displays evidence of pervasive sand fluidisation caused by
339 fluid ingress and increased pore-fluid pressure. The most intense fluidisation
340 occurred in the upper portion of the sandstone as shown by the irregular shape of
341 the top surface. Most Type 1 SFNF occur where the sandstone pinches out. Here,
342 the limited thickness of the sandstone allowed lateral sand evacuation, which in turn
343 caused the failure of the overburden, and the successive injection of the fluidized
344 sand along faults (Fig. 6a, b). A fundamental characteristic of the outcrop is that
345 sandstone-filled structures only develop above the remobilized sandstone. SFNF do
346 not transect the depositional sandstone, as shown by the undeformed basal surface.
347 This is a diagnostic criteria that allows differentiation between Types 1 and 2 SFNF.

348 Type 2b SFNF recognized in the outcrop O2 form conjugate sets that have
349 sandstone-filled apertures ranging from a few centimetres to some tens of
350 decimetres, and offsets varying from a few decimetres to metres (Fig. 7a, b). Fault
351 spacing varies from a few decimetres to several metres. Injected sandstone displays
352 laminations parallel to the fault wall, and this is the only internal characteristic
353 present. Mudstone clasts, together with slightly cemented sandstone belonging to
354 the host strata are quite common within the sand injection. Kinematic indicators as
355 well as slickensides are locally preserved, although they tend to be removed during
356 the sandstone emplacement process. Evidence of pre-existing fault gouge is very
357 rare. In most cases, faults display planar surfaces, although local curvatures giving

358 rise to releasing steps and dilational jogs, are sometimes present. The effects of
359 post-emplacement compaction are preserved as segmentation of dikes and fault-
360 plane curvature. WSW-ENE trending Type 2b SFNF (Fig. 7c) recognized in the
361 outcrop O2, are consistent with outer arc extensional faults recognized in the Tumey
362 Gulch area (Palladino et al., 2016).

363

364 5.2. *Monocline Ridge*

365 Monocline Ridge is a NE-dipping monocline situated along the western side of
366 the San Joaquin Valley (Fig. 1a). Numerous well preserved outcrops of Type 1 SFNF
367 are present along this structure. Outcrop O3 (Fig. 8a, b) consists of a SW-dipping
368 array of sandstone-filled reverse faults and Type 1 SFNF cutting through the
369 Kreyenhagen Shale. The occurrence in this area of sandstone-filled contractional
370 structures was documented by Palladino et al. (2016). SFNF have apertures of some
371 centimetres and offsets of a few tens of centimetres. Neither fault gouge nor
372 kinematic indicators are preserved along the fault surface. Rare cm-scale mudstone
373 clasts 'float' in the sand matrix. In Fig. 8b, Fault 1 consists of a single fault surface
374 filled with an almost constant thickness of sandstone, while Fault 2 is a composite
375 fault comprising different lozenge-shaped, *en echelon*, sandstone-filled segments.

376

377 5.3. *Panther Beach*

378 Well-preserved Type 2a SFNF are exposed along the entire coastal section
379 between Santa Cruz and Davenport (Fig. 1b). A key example is represented by
380 Outcrop O4 at Panther Beach (Fig. 9a, b). This outcrop consists of a NE-SW

381 oriented SFNF (Fig. 9c) that cuts the diatomaceous Santa Cruz Mudstone. The fault
382 plane is strongly undulose, fault throw is ~10 cm and fault aperture ranges between
383 1 and 5 cm. Fault zone thickness is significantly reduced and fault gouge is almost
384 absent while remobilized sand fully fills the fault zone. Where the fault cuts the
385 mudstone marker bed, slight clay smear occurs and sandstone infill loses its
386 continuity.

387

388 **6. Mechanisms driving emplacement of sand injections along normal faults**

389 Fluidized sand can be intruded along normal fault planes as a result of two
390 main mechanisms: i) fluidized sand sourced from an over-pressured unit lift the
391 overburden causing hydrofracturing of the host strata and forced filling (propping) of
392 the newly-formed fault. In this case, fault generation is triggered by overpressure and
393 the sand is intruded into the newly-formed faults. Type1 SFNF are the result of this
394 process; ii) overpressured fluidized sand fills low-pressure voids developed along a
395 fault plane. Failure in host strata is not solely associated with overpressure but
396 rather, to external factors such as regional tectonics. Type 2 SFNF typically originate
397 by this process.

398 Sand injection occurs along a newly-formed fault or, exploits a pre-existing
399 discontinuity (fault or fracture). Exploitation of pre-existing faults depends upon the
400 degree of cohesion and cementation of the tectonically-generated structure and,
401 whether pore-fluid overpressure (P_f) exceeds the lithostatic overburden and the
402 tensile stress associated with opening of the fracture plane. Commonly, sand
403 fluidisation into open structures is predominantly in the upper (200-500 m) sub-

404 surface within poorly-consolidated and only lightly compacted strata (Vigorito and
405 Hurst, 2010; Hurst et al., 2011).

406

407 *6.1. Emplacement of sand injections along Type 1 SFNF*

408 Type 1 SFNF typically breach the overburden of a poorly-consolidated
409 sandstone body (either a pristine depositional unit or a pre-existing sandstone
410 intrusion) when P_f exceeds the fracture gradient of the overburden (Fig. 10a). In
411 order to achieve this, rapid ingress of pore-fluid is required to initiate hydraulic
412 fracture and sand fluidisation. As overpressure is build, for example when a dike
413 connects a sandstone with deeper overpressured units, sand grain fluidization is
414 initiated and sand begins to mobilise into the fault (Fig. 10a). In particular, where the
415 dike connects with the sandstone and new sand is added to the system, the
416 overpressured sand body will show important modifications in the shape, as well as
417 irregular top surfaces and scallops (Hurst et al., 2011). Concurrently, as the pore-
418 fluid pressure exceeds the fracture gradient of the overburden plus its tensile
419 strength, a hydrofractured belt consisting of faults and fractures forms in the host
420 strata along the top of the sandstone body from which sand is being fluidised. Then,
421 fluidized sand, driven upward by buoyant force, begins to flow toward lower-
422 pressured zones represented by the overlying mechanical discontinuities.
423 Immediately after, the lateral evacuation of sand from necked zones can cause the
424 further collapse of the overburden, already weakened by the formation of the
425 hydrofractures, which is accommodated by further faulting and fracturing (Fig. 10b).
426 Dilation along normal faults and fractures, sustained by the fluid overpressure,
427 favours the emplacement of fluidized sand within the newly-formed structures.

428

429 *6.2. Emplacement of sand injections along Type 2 SFNF*

430 Faults that intersect an isolated over-pressured sandstone (Fig. 10c)
431 determine the location of the rupture of the surrounding low impermeability host

432 strata by causing a sudden disturbance in the fluid pressure. Specifically, as a fault is
433 a low pressure zone relative to the sandstone unit, a pressure gradient with flow
434 directed toward the fault surface develops instantaneously (Fig. 10d). The resulting
435 discharge of fluid results in an abrupt drop of P_f in the sandstone, a process that
436 continues until the hydrostatic gradient is restored (Sibson, 1990; 1992). Under
437 certain circumstances, the influx of high-pressured water into the fault zone can have
438 a two-fold effect: i) if P_f exceeds the overburden pressure present in the hangingwall
439 block, it contributes to prop open the newly-formed discontinuity; ii) If the movement
440 of the pore fluid produced during pressure equilibration exceeds the minimum
441 fluidization velocity of sand (for example equal to 0.3-1 cm/s for well-sorted, fine-
442 grained sands), it imposes a drag force that mobilizes sand grains. In such a
443 situation, poorly-lithified sandstone begins to fluidize and injects into cavities along
444 the fault plane (Fig. 10e). In cases where faulting is triggered by the remobilization
445 process (see the previous section), the origin and distribution of the newly-formed
446 extensional faults within an undisturbed and homogeneous top seal is controlled by
447 the stress field acting around the overpressured sandstone. In this case, for a fault to
448 be propped open, pore pressure (P_f) must exceed the minimum principal stress (σ_3)
449 plus the tensile strength (T): $P_f > \sigma_3 + T$.

450

451 **7. Discussion**

452 *7.1. Favourable conditions for SFNF emplacement*

453 Although normal faults developed in the PGIC, TGIC and the SCIC display
454 differences related to the structure of damage zones (Fig. 3), they all frequently host
455 sandstone intrusions. It is thus important to understand the conditions that promote

456 sand emplacement into such a diverse range of structures. As discussed previously,
457 the emplacement of remobilized sand along a fault is strictly related to the ascent of
458 fluids from a source of high fluid-pressure located deeper in the faulted succession.
459 Depending on the state of fracturing in the host strata, the fluid ingress is either
460 focussed along the fault zone, or dissipated into adjacent strata thereby losing the
461 potential to fluidize sand. Obviously, the emplacement of SFNF is strictly related to
462 the first scenario.

463 In poorly-consolidated strata, such as the Panoche/Tumey-type successions
464 (Fig. 3a), which are characterized by ductile behaviour and low fault-parallel
465 secondary permeability, the ascending over-pressured fluid is hindered by obstacles
466 such as mudstone units, whereas fluid transfer is facilitated along vertical conduits
467 represented by faults (Fig. 3b). In addition, the characteristic of poorly-consolidated,
468 finely interbedded mudstone and sandstone, fault-related deformational
469 mechanisms, such as dragging, ductile flow and clay smear all contribute toward the
470 formation of narrow damage zones and an inner fault-parallel layering, which forces
471 fluid to move along the fault zone. Consequently SFNF is widespread in the PGIC
472 and TGIC, and locally forms closely-spaced swarms (Figs. 7-8).

473 In well-consolidated host rock, such as the Santa Cruz type succession (Fig.
474 3c), the development of high fault-parallel secondary permeability, favoured by the
475 brittle behaviour of the deformed rocks, does not typically permit sandstone intrusion
476 along faults. However, even under these unfavourable conditions, the injection of
477 sand along isolated fault planes occurs. As the width of the fault damage zone in this
478 succession is directly proportional to the amount of the fault displacement,
479 sandstone intrusion is still possible where small displacements occur (Fig. 9). Faults

480 with small offsets do not have space to develop a complete fault zone, such that the
481 core zone is almost absent and the damage zone is poorly-developed.

482

483 *7.2. Cross-cutting relationships*

484 Type 1 and Type 2 SFNF consist of very similar structures generated by very
485 different processes described in the previous sections. Commonly, the processes
486 creating these two types of structures are unrelated, but in specific circumstances it
487 is possible that Type 1 SFNF and Type 2 SFNF coexist. In our examples their
488 coexistence implies formation, at different times, with the time of sand injection
489 separated by ~20 Ma (Fig. 11). In particular, Type 1 SFNF formed concurrently with
490 the emplacement of the main sand injection complexes (PGIC, TGIC and SCIC) and
491 their age is the same as the hosting complex. Type 2 SFNF, although also
492 associated with these complexes, represent a younger tectonically-controlled
493 sandstone intrusion event that postdates the emplacement of the main injection
494 complexes. Evidence for Type 2 SFNF overprinting older sand injection complexes
495 in central California are demonstrated by cross-cutting relationships described in the
496 following sections.

497

498 *7.2.1. Panoche/Tumey hills*

499 In the Panoche/Tumey hills area, Type 2 SFNF represent an episode of sand
500 injection that post-dates the emplacement of PGIC, TGIC and Type 1 SFNF (Fig. 1).
501 Clear evidence of these relationships is observed throughout the study area and in
502 particular along Monocline Ridge (Fig. 2).

503 The outcrop O5 (Fig. 12a, b) shows a set of mesoscale, WNW-ESE oriented
504 conjugate Type 2 SFNF (Fig. 12c) that dissect the Kreyenhagen Shale , together
505 with an older generation of cm- to dm-thick, tabular, sandstone intrusions belonging
506 to the TGIC. Fault displacement commonly ranges from a few millimetres to several
507 centimetres, while apertures vary from a few centimetres to tens of decimetres. Sand
508 intruded along fault planes appear to be directed both upwards and downwards (Fig.
509 12d). However, the occurrence of fragments of the host strata unrelated to the fault
510 walls leads us to believe that lateral transport was also possible. It is interesting to
511 note that sand remobilization mainly occurs along the fault segments that are located
512 immediately above and below the deformed sandstone units. Within the faulted
513 sandstone, no evidence of sand fluidization is preserved and the presence of the
514 fault plane is marked by the occurrence of deformation bands (Fig. 12e). In this case,
515 sand fluidization only occurred along the margins of the sandstone at the contact
516 with the host strata, whereas the inner portion was unaffected.

517

518 *7.2.2. Santa Cruz area*

519 In the Santa Cruz area (Fig. 2), Type 2 SFNF clearly dissect an older
520 generation of sandstone intrusions belonging to the SCIC (Fig. 13). Outcrop O4, at
521 the southern end of Panther Beach, 10 km west of Santa Cruz, consists of a cliff
522 composed of diatomaceous mudstone and a few cm-scale tar-saturated, low-angle
523 dikes, which are repeatedly cut by a series of conjugate faults with cm-scale offsets
524 (Fig. 13a, b). Here, a well-preserved example of a WNW-ESE-trending Type 2a
525 SFNF has an offset of 15 cm and cuts a low-angle dike (Fig. 13c). In detail, the fault
526 plane consists of bifurcating and anastomosing fault segments and fractures

527 connected by damage-zone linkages. Extensional steps and dilational jogs are very
528 common and are a diagnostic record of brittle deformation in the mudstone. The
529 faulted sandstone displays hangingwall and footwall drag folds, and a progressive
530 increase in the number of fractures toward the damage zone. Along some of the fault
531 segments, sandstone intrusions generated by the partial fluidization of the deformed
532 dike are observed. In particular, the segment of the dike located in the hangingwall
533 bifurcates, with one branch connecting with the sandstone in the footwall, while
534 another branch intrudes upward along the tectonic discontinuity (Fig. 13b). Sand
535 fluidization and lateral sand evacuation processes may explain the observed thinning
536 of the dike in the fault zone.

537

538 *7.3 Implications for reservoir connectivity*

539 The distribution and transmissibility of fluids within reservoirs is strongly
540 affected by the presence of faults that act either as conduits or barriers to fluid flow
541 (Child et al., 1997; Knipe, 1997; Manzocchi et al., 1998; Aydin, 2000; Bailey et al.,
542 2002; Faulkner et al., 2010). Occurrence of injected sand along fault planes forming
543 the SFNF, has significant effect on enhancing and perpetuating cross- and along-
544 fault permeability in otherwise poorly-connected siliciclastic strata. In the light of our
545 outcrop observations, it appears that most SFNF displacements occur below the
546 resolution of seismic data typical of oilfield locations. Lack of resolution of these fault-
547 related sandstones compromises the appraisal of the volume of strata within which
548 permeable, connected reservoir volume exists. In practice this can lead to
549 substantial underestimation of hydrocarbon recovery if the presence and significance
550 of SFNF remain unidentified.

551 Recognition of SFNF is particularly important for reservoirs with
552 Panoche/Tumey-type successions (Fig. 3). Because of juxtaposition between
553 reservoir and non-reservoir facies, and the formation of a low permeability gouge,
554 faults that dissect Panoche/Tumey-type successions are likely to behave as
555 hydraulic barriers that reduce cross-fault fluid flow (Rawling et al., 2001; Bense et al.,
556 2003; Caine and Minor, 2009) (Fig. 14a). Occurrence of SFNF in these types of
557 successions may provide enhanced connectivity between sandstone that are
558 otherwise displaced by faults (Fig. 14b). If clay smear and fine-grained cataclastic
559 material are present along fault walls this may be eroded by turbulent granular flow
560 during sand fluidization and injection thus enhancing connectivity across a fault
561 plane (Fig. 14c). Fault-strike and fault-dip modifications of faults during sand injection
562 and by the emplacement of sandstone intrusions favour connectivity in reservoir
563 intervals.

564 Reservoirs with a Santa Cruz -type succession (Fig. 3), generally have faults
565 that produce fracture permeability which prevent the emplacement of sand along
566 normal faults. However, where this type of succession is characterized by low
567 deformation, isolated normal faults with small offsets may host injected sand. This
568 makes a strong contribution to enhanced gross permeability of non-reservoir strata
569 by enhancing the permeable network and new conduits for fluid migration.

570 Arrays of SFNF that cuts through sub-horizontal sandstone are expected to
571 give rise to meso- and large-scale wing-like and conical sandstone intrusions, which
572 should not be confused with those emplaced in the absence of tectonic influence
573 (Huuse et al., 2007). In particular, parallel arrays of constantly dipping SFNF can be
574 responsible for the formation of stepped sills (Fig. 15a, b), while conjugate sets of
575 SFNF may give rise to saucer-shaped and conical geometries (Fig. 15c, d).

576 Structurally-controlled wing-like sandstone intrusions can be identified in seismic
577 sections as they lack the characteristic jack-up that lifts beds that overlie sandstone
578 intrusion (Szarawarska et al., 2010). Despite having structurally- and non-
579 structurally-controlled sandstone intrusions that display broadly similar geometry, it is
580 crucial to discriminate between the two categories when evaluating the behaviour of
581 subsurface fluid migration. SFNF may have specific reliance to planning and
582 optimizing hydrocarbon recovery by influencing fluid distribution in hydrocarbon
583 reservoirs. By contrast, SFNF may represent a persistent open drainage (seal-
584 breach) through which fluids continuously leak thereby limiting hydrocarbon
585 accumulation and generally facilitating ease of drainage of all basin-derived fluids
586 (Cartwright et al., 2007).

587 The occurrence of SFNF in a hydrocarbon reservoir can significantly increase
588 the general connectivity. Under favourable conditions, this result in enhanced
589 permeability and an increase in the reservoir rock volume. However, with
590 unfavourable conditions, SFNF can promote considerable hydrocarbon leakage by
591 connecting reservoir rocks with either the topographic surface or other permeable
592 horizons in the stratigraphic succession.

593

594 **8. Summary and conclusions**

595 Details of sand-filled normal faults (SFNF) recognized from two areas in
596 central California, in which contrasting normal fault characteristics associated with
597 larger sand injection complexes are present, are documented for the first time in this
598 paper. SFNF were intruded into Late Cretaceous and Eocene host strata in the
599 Panoche/Tumey hills, and in Miocene strata along the coast north of Santa Cruz.

600 Two main SFNF types are recognized: i) Type 1 SFNF form in response to the
601 rapid increase of pore fluid over-pressure in poorly-consolidated sandstone, and the
602 consequent hydraulic failure of the overlying host strata; ii) Type 2 SFNF form as a
603 consequence of regional tectonic deformation, and the resulting draining of fluidized
604 sand toward the tectonic structures.

605 SFNF occur in host strata that are either poorly-consolidated, as in the case of
606 Panoche/Tumey-Type successions, or well-consolidated, as in the Santa Cruz
607 examples. Development of sand-filled normal faults is more likely in the first case
608 due the ductile behaviour of the deformed strata. SFNF in the Santa Cruz strata are
609 far less common and form only where limited fault throw occurs and within poorly-
610 developed fault core zones.

611 The recognition of SFNF is crucial when enhancing the understanding of
612 subsurface fluid migration in the very shallow crust and when associated with
613 hydrocarbon reservoirs. Although the structures we describe are below seismic
614 resolution, they form a permeable network, with fluidized sand acting as a natural
615 proppant that increases the connectivity of reservoirs even in adverse geological
616 conditions. SFNF are thus a new element that must be added to the conventional
617 methods of fault seal analysis and in particular when developing reservoir where
618 sandstone intrusions are present.

619

620 **Acknowledgments**

621 We acknowledge the support of sponsoring companies of Phase 3 of the Sand
622 Injection Research Group (SIRG). We would like to thank Chris Morley and another

623 anonymous reviewer for constructive comments, and the editor for efficient handling
624 of this paper. We also wish to thank and acknowledge the continuing help and
625 access provided by the Bureau of Land Management and in particular Greg
626 Middleton without whose enthusiasm and support our research would have been
627 much more challenging.

628

629 **References**

630 Ainsworth, R.B., 2006. Sequence stratigraphic-based analysis of reservoir
631 connectivity: Influence of sealing faults – a case study from a marginal marine
632 depositional setting. *Petroleum Geoscience* 12, 127–141.

633 Atwater, T., Stock, J., 1998. Pacific-north America plate tectonics of the Neogene
634 southwestern United States: an update. *International Geology Review* 40, 375-402.

635 Aydin, A., Page, B.M., 1984. Diverse Pliocene-Quaternary tectonics in a transform
636 environment, San Francisco Bay region, California. *Geological Society of America*
637 *Bulletin* 95, 1303-1317.

638 Aydin, A., 2000. Fractures, faults, and hydrocarbon entrapment, migration and flow.
639 *Marine and Petroleum Geology* 17, 797-814.

640 Audemard, F.A., de Santis, F., 1991. Survey of liquefaction structures induced by
641 recent moderate earthquakes. *Bulletin of Engineering Geology and the Environment*
642 44, 5-16.

643 Bailey, W.R., Manzocchi, T., Walsh, J.J., Strand, J.A., Nell, P.A., Keogh, K.,
644 Hodgetts, D., Flint, S., Rippon, J., 2002. The effects of faults on the 3-D connectivity

645 of reservoir bodies: a case study from the East Pennine Coalfield, UK. *Petroleum*
646 *Geoscience* 8, 263–277.

647 Ballas, G., Fossen, H., Soliva, R., 2015. Factors controlling permeability of
648 cataclastic deformation bands and faults in porous sandstone reservoirs. *Journal of*
649 *Structural Geology* 76, 1-21.

650 Barron, J.A., 1986. Paleooceanographic and tectonic controls on deposition of the
651 Monterey Formation and related siliceous rocks in California. *Palaeogeography,*
652 *Palaeoclimatology, Palaeoecology* 53, 27-45.

653 Bartow, J.A., 1991. The Cenozoic evolution of the San Joaquin valley California.
654 USGS Geological Survey Professional Paper 1501, 40p.

655 Bartow, J.A., 1996. Geological Map of the West Border of the San Joaquin Valley in
656 the Panoche Creek-Cantua Creek Area, Fresno and San Benito Counties, California:
657 Miscellaneous Investigations Series-US Geological Survey Map I-2430, Scale
658 1:50000.

659 Bense, V.F., Van den Berg, E.H., Van Balen, R.T., 2003. Deformation mechanisms
660 and hydraulic properties of fault zones in unconsolidated sediments; the Roer Valley
661 Rift System, the Netherlands. *Hydrogeology Journal* 11, 319–332.

662 Bense, V., van Balen, R., 2003. Hydrogeological aspects of fault zones on various
663 scales in the Roer Valley Rift System. *Journal of Geochemical Exploration* 78-79,
664 317-320.

665 Bense, V. F., Person, M.A., 2006. Faults as conduit-barrier systems to fluid flow in
666 siliciclastic sedimentary aquifers. *Water Resources Research* 42, W05421,
667 doi:10.1029/2005WR004480.

668 Boehm, A., Moore, J.C., 2002. Fluidized sandstone intrusions as an indicator of
669 paleostress orientation, Santa Cruz, California. *Geofluids* 2, 147-161.

670 Braathen, A., Tveranger, J., Fossen, H., Skar, T., Cardozo, N., Semshaug, S.E.,
671 Bastesen, E., Sverdrup, E., 2009. Fault facies and its application to sandstone
672 reservoirs. *AAPG Bulletin* 93, 891–917.

673 Bureau, D., Mourgues, R., Cartwright, J., Foschi, M., Abdelmalak, M.M., 2013.
674 Characterisation of interactions between a pre-existing polygonal fault system and
675 sandstone intrusions and the determination of paleo-stresses in the Faroe-Shetland
676 basin. *Journal of Structural Geology* 46, 186-199.

677 Caine, J.S., Evans, J.P., Forster, C.B., 1996. Fault zone architecture and
678 permeability structure. *Geology* 24, 1025–1028.

679 Caine, J.S., Minor, S.A., 2009. Structural and geochemical characteristics of faulted
680 sediments and inferences on the role of water in deformation, Rio Grande Rift, New
681 Mexico. *GSA Bulletin* 121, 1325–1340.

682 Cartwright, J., Huuse, M., Aplin, A., 2007. Seal bypass systems. *AAPG Bulletin* 91,
683 1141–1166.

684 Childs, C., Walsh, J.J., Watterson, J., 1997. Complexity in fault zone structure and
685 implications for fault seal prediction. In: Møller-Pedersen, P., Koestler, A.G. (Eds.),
686 *Hydrocarbon Seals: Importance for Exploration and Production*. NPF Special
687 Publication 7, Elsevier, Singapore, 61-72.

688 Childs, C., Walsh, J.J., Manzocchi, T., Strand, J., Nicol, A., Tomasso, M., Schöpfer
689 M.P.J., Aplin, A.C., 2007. Definition of a fault permeability predictor from outcrop
690 studies of a faulted turbidite sequence, Taranaki, New Zealand. In: Jolley, S.J., Barr,

691 D., Walsh, J.J., Knipe, R.J. (Eds.), Structurally Complex Reservoirs. Geological
692 Society, London, Special Publications, 292, 235–258.

693 Childs, C., Manzocchi T., Walsh, J.J., Bonson, C.G., Nicol, A., Schöpfer, M.P.J.,
694 2009. A geometric model of fault zone and fault rock thickness variations. Journal of
695 Structural Geology 31, 117-127.

696 Clark, J.C., 1981. Stratigraphy, palaeontology, and geology of the central Santa Cruz
697 Mountains, California Coast Range: U.S. Geological Survey Professional Paper
698 1168, p. 51.

699 Constenius, K.N., Johnson, R.A., Dickinson, W.R., Williams, T.A., 2000. Tectonic
700 evolution of the Jurassic-Cretaceous Great Valley forearc, California: implications for
701 the Franciscan thrust-wedge hypothesis. G S A Bulletin 112, 1703-1723.

702 Dickinson, W.R., Seely, D.R., 1979. Structure and stratigraphy of forearc regions.
703 AAPG Bulletin 63, 2-31.

704 Dixon, R.J., Schofield, K., Anderton, R., Reynolds, A.D., Alexander, R.W.S.,
705 Williams, M.C., Davies, K.G., 1995. Sandstone diapirism and clastic intrusion in the
706 Tertiary submarine fans of the Bruce-Beryl Embayment, Quadrant 9, UKCS. In:
707 Hartley, A.J., Prosser, D.J. (Eds.), Characterisation of deep-marine clastic systems:
708 Special Publication 94. Geological Society, London, 77–94.

709 Dumitru, T.A., 1989. Constraints on uplift in the Franciscan subduction complex from
710 apatite fission track analysis. Tectonics 8, 197-220.

711 Faulkner, D.R., Jackson, C.A.L., Lunn, R.J., Schlische, R.W., Shipton, Z.K.,
712 Wibberley, C.A.J., Withjack, M.O., 2010. A review of recent developments

713 concerning the structure, mechanics and fluid flow properties of fault zones. *Journal*
714 *of Structural Geology* 32, 1557-1575.

715 Fredman, N., Tveranger, J., Semshaug, S., Braathen, A., Sverdrup, E., 2007.
716 Sensitivity of fluid flow to fault core architecture and petrophysical properties of fault
717 rocks in siliciclastic reservoirs: a synthetic fault model study. *Petroleum Geoscience*,
718 13, 1–16.

719 Gross, M.R., Becker, A., Gutiérrez-Alonso, G., 1997. Transfer of displacement from
720 multiple slip zones to a major detachment in an extensional regime: Example from
721 the Dead Sea rift, Israel. *GSA Bulletin* 109, 1021–1035.

722 Harms, T.A., Jayko, A.S., Blake, M.C., 1992. Kinematic evidence for extensional
723 unroofing of the Franciscan complex along the Coast Range Fault, northern Diablo
724 Range, California. *Tectonics* 11, 228-241.

725 Heynekamp, M.R., Goodwin, L.B., Mozley, P.S., Haneberg, W.C., 1999. Controls on
726 fault zone architecture in poorly lithified sediments, Rio Grande rift, New Mexico:
727 Implications for fault-zone permeability and fluid flow. In: Haneberg, W.C., Mozley,
728 P.S., Moore, J.C., Goodwin, L.B. (Eds.), *Faults and subsurface fluid flow in the*
729 *shallow crust: American Geophysical Union Monograph* 113, 27–49.

730 Hurst, A., Cartwright, J.A., Huuse, M., Duranti, D., 2006. Extrusive sandstones
731 (extrudites): a new class of stratigraphic trap? In: Allen, M.R., Goffey, G.R, Morgan,
732 R.K., Walker, I.M. (Eds.), *The deliberate search for the stratigraphic trap. Geological*
733 *Society, London, Special Publications* 254, 289-300.

734 Hurst, A., Scott, A., Vigorito, M., 2011. Physical characteristics of sand injectites.
735 *Earth Science Reviews* 106, 215-246.

736 Huuse, M., Cartwright, J., Hurst, A., Steinsland, N., 2007. Seismic characterization of
737 large-scale sandstone intrusions. In: Hurst, A., Cartwright, J., (Eds.), Sand injectites:
738 Implications for hydrocarbon exploration and production: AAPG Memoir 87, 21-35.

739 Ingersoll, R.V., 1979. Evolution of the Late Cretaceous forearc basin, northern and
740 central California. GSA Bulletin 90, 813-826.

741 Johnson, C.L., Graham, S.A., 2007. Middle Tertiary Stratigraphic Sequences of the
742 San Joaquin Basin, California. In: Petroleum Systems and Geologic Assessment of
743 Oil and Gas in the San Joaquin Basin Province, California. Hosford Scheirer, Allegra,
744 Ed., 2007, U.S. Geological Survey Professional Paper 1713.

745 Jolley, S.J., Barr, D., Walsh, J.J., Knipe, R.J., 2007. Structurally complex reservoirs:
746 an introduction. In: Jolley, S. J., Barr, D., Walsh, J. J. Knipe, R. J. (Eds.), Structurally
747 Complex Reservoirs. Geological Society, London, Special Publications 292, 1–24.

748 Jolly, R.J.H., Lonergan, L., 2002. Mechanisms and controls on the formation of sand
749 intrusions. Journal of the Geological Society, London 159, 605-617.

750 Jones, G., Fisher, Q.J., Knipe, R.J. (Eds.), 1998. Faulting, fault sealing and fluid flow
751 in hydrocarbon reservoirs. Geological Society, London, Special Publications 147.

752 Jonk, R., Duranti, D., Parnell, J., Hurst, A., Fallick, A.E., 2003. The structural and
753 diagenetic evolution of injected sandstones: examples from the Kimmeridgian of NE
754 Scotland. Geological Society of London 160, 881–894.

755 Kim, Y., Peacock, D.C.P., Sanderson, D.J., 2004. Fault damage zones. Journal of
756 Structural Geology 26, 503-517.

757 Knipe, R.J., 1997, Juxtaposition and seal diagrams to help analyze fault seals in
758 hydrocarbon reservoirs. AAPG Bulletin 81, 187-195.

759 Knipe, R.J., Jones, G., Fisher, Q.J., 1998. Faulting, fault sealing and fluid flow in
760 hydrocarbon reservoirs: an introduction. In: Jones, G., Fisher, Q.J., Knipe, R.J.
761 (Eds.) Faulting, Fault Sealing and Fluid Flow in Hydrocarbon Reservoirs. Geological
762 Society, London, Special Publications, 147, 7-21.

763 Knott, S.D., Beach, A., Brockbank, P.J., Brown, J.L., McCallum, J.E., Welbon, A.I.,
764 1996. Spatial and mechanical controls on normal fault populations. Journal of
765 Structural Geology 18, 359-372.

766 Koša, E., 2007. Differential subsidence driving the formation of mounded
767 stratigraphy in deep-water sediments; Palaeocene, central North Sea. Marine and
768 Petroleum Geology 24, 632-652.

769 Krueger, S.W., Jones, D.L., 1989. Extensional fault uplift of regional Franciscan
770 blueschists due to subduction shallowing during the Laramide orogeny. Geology 17,
771 1157-1159.

772 Lewis, G., Knipe, R.J., Li, A., 2002. Fault seal analysis in unconsolidated sediments:
773 a field study from Kentucky, USA. In: Koestler, A.G., Hunsdale, R., (Eds.),
774 Hydrocarbon Seal Quantification. NPF Special Publication 11, Elsevier Science B.V.,
775 Amsterdam, 243-253.

776 Loveless, S., Bense, V., Turner, J., 2011. Fault architecture and deformation
777 processes within poorly lithified rift sediments, Central Greece. Journal of Structural
778 Geology 33, 1554-1568.

779 Lowe, D.R., 1975. Water escape structures in coarse-grained sediments.
780 *Sedimentology* 22, 157–204.

781 Manzocchi, T., Ringrose, P.S., Underhill, J.R., 1998. Flow through fault systems in
782 high-porosity sandstones. In: Coward, M.P., Daltaban, T.S., Johnson, H. (Eds.),
783 *Structural Geology in Reservoir Characterization*. Geological Society, London,
784 *Special Publications* 127, 65-82.

785 Manzocchi, T., Walsh, J.J., Nell, P., Yielding, G., 1999. Fault transmissibility
786 multipliers for flow simulation models. *Petroleum Geoscience* 5, 53-63.

787 Montenat, C., Barrier, P., Ott d'Estevou, P., Hibsich, C., 2007. Seismites: An attempt
788 at critical analysis and classification. *Sedimentary Geology* 196, 5–30.

789 Moxon, I.W., 1988. Sequence stratigraphy of the Great Valley basin in the context of
790 convergent margin tectonics. In: Graham, S.A. (Ed.), *Studies of the Geology of the*
791 *San Joaquin Basin, Pacific Section, Society of Economic Paleontologists and*
792 *Mineralogists* 60, 3-28.

793 Namson, J.S., Davis, T.L., 1988. Seismically active fold and thrust belt in the San
794 Joaquin Valley, central California. *GSA Bulletin* 100, 257-273.

795 Page, B.M., Thompson, G.A., Coleman, R.G., 1998. Late Cenozoic tectonics of the
796 central and southern coast ranges of California. *GSA Bulletin* 110, 846-876.

797 Palladino, G., Grippa, A., Bureau, D., G. Ian, Alsop, Hurst, A., 2016. Emplacement of
798 sandstone intrusions during contractional tectonics. *Journal of Structural Geology* 89,
799 230-249.

800 Peacock, D.C.P., Dimmen, V., Rotevatn, A., Sanderson, D.J., 2017. A broader
801 classification of damage zones. *Journal of Structural Geology*. doi:
802 10.1016/j.jsg.2017.08.004.

803 Phillips, R.L., 1990. Depositional and structural controls on the distribution of tar
804 sands in the Santa Cruz mountains, California. In: Garrison, R, Greene, H.G., Hicks,
805 K.R., Weber, G.E., Wright, T.L. (Eds.), *Geology and Tectonics of the Central*
806 *California Coastal Region, San Francisco to Monterey, Volume and Guidebook,*
807 *Pacific Section, American Association of Petroleum Geologists, Pacific Section,*
808 *Bakersfield, CA, Book GB67, 105–21.*

809 Ravier, E., Guiraud, M., Guillien, A., Vennin, E., Buoncristiani, J.F., Portier, E., 2015.
810 Micro- to macro-scale internal structures, diagenesis and petrophysical evolution of
811 injectite networks in the Vocontian Basin (France): Implications for fluid flow. *Marine*
812 *and Petroleum Geology* 64, 125-151.

813 Rawling, G.C., Goodwin, L.B., Wilson, J.L., 2001. Internal architecture, permeability
814 structure, and hydrologic significance of contrasting fault-zone types. *Geology* 29,
815 43-46.

816 Ribeiro, C., Terrinha, P., 2007. Formation, deformation and chertification of
817 systematic clastic dykes in a differentially lithified carbonate multilayer. SW Iberia,
818 Algarve Basin, Lower Jurassic. *Sedimentary Geology* 196, 201–215.

819 Shoulders, S.J., Cartwright, J., Huuse, M., 2007. Large-scale conical sandstone
820 intrusions and polygonal fault systems in Tranche 6, Faroe-Shetland Basin. *Marine*
821 *and Petroleum Geology* 24, 173–188.

822 Scott, A., Vigorito, M., Hurst, A., 2009. The process of sand injection: internal
823 structures and relationships with host strata (Yellowbank Creek Injectite Complex,
824 California, U.S.A.). *Journal of Sedimentary Research* 79, 568–583.

825 Scott, A., Hurst, A., Vigorito, M., 2013. Outcrop-based reservoir characterization of a
826 kilometer-scale sand-injectite complex. *AAPG Bulletin* 97, 309-343.

827 Sharman, G.R., Graham, S.A., Grove, M., Hourigan, J.K., 2013. A reappraisal of the
828 early slip history of the San Andreas fault, central California, USA. *Geology* 41, 727-
829 730.

830 Sibson, R.H., 1990. Conditions for fault-valve behaviour. In: Knipe, R.J., Rutter, E.H.
831 (Eds.), *Deformation Mechanisms, Rheology and Tectonics*. Geological Society,
832 London, Special Publications 54, 15-28.

833 Sibson, R.H., 1992. Implications of fault valve behaviour for rupture nucleation and
834 recurrence. *Tectonophysics* 211, 283-293.

835 Siddoway, C.S., Gehrels G.E., 2014. Basement-hosted sandstone injectites of
836 Colorado: A vestige of the Neoproterozoic revealed through detrital zircon
837 provenance analysis. *Lithosphere* 6, 403–408.

838 Siddoway, C.S., Prosser, G. Palladino, G., 2017. Sandstone intrusions in fractured
839 crystalline basement: implication for hydrocarbon reservoir connectivity. In: Hurst A.,
840 Silcock, S., Dennis, H., Huuse M., Lovelock, C., Wild, J. (Eds.), *Subsurface sand*
841 *remobilization and injection: implication for oil and gas exploration and development*.
842 The geological Society, London, 85-86.

843 Sousa, F.J., Farley, K.A., Saleeby, J., Clark, M., 2016. Eocene activity on the
844 Western Sierra Fault System and its role incising Kings Canyon, California. *Earth
845 and Planetary Science Letters* 439, 29–38.

846 Sperrevik, S., Gillespie, P.A., Fisher, Q.J., Halvorsen, T., Knipe, R.J., 2002.
847 Empirical estimation of fault rock properties. In: Koestler, A.G., Hunsdale, R. (Eds.)
848 *Hydrocarbon Seal Quantification*. NPF Special Publication 11, 109-125. Elsevier,
849 Amsterdam.

850 Szarawarska, E., Huuse, M., Hurst, A., de Boer, W., Lu, L., Molyneux, S., Rawlinson,
851 P., 2010. Three-dimensional seismic characterisation of large-scale sandstone
852 intrusions in the lower Palaeogene of the North Sea: completely injected vs. in situ
853 remobilised sandbodies. *Basin Research* 22, 517–532.

854 Taylor, B.J., 1982. Sedimentary dykes, pipes and related structures in the Mesozoic
855 sediments of south-eastern Alexander Island. *British Antarctic Survey Bulletin* 51, 1-
856 42.

857 Thompson, B.J., Garrison, R.E., Moore, C.J., 1999. A late Cenozoic sandstone
858 intrusion west of S. Cruz, California. Fluidized flow of water and hydrocarbon-
859 saturated sediments. In: Garrison, R.E., Aiello, I.W., Moore, J.C. (Eds.), *Late
860 Cenozoic Fluid Seeps and Tectonics along the San Gregorio Fault Zone in the
861 Monterey Bay Region, California GB-76*. Annual Meeting of the Pacific Section.
862 American Association of Petroleum Geologists, Monterey, California, 53–74.

863 Thompson, B.J., Garrison, R.E., Moore, C.J., 2007. A reservoir-scale Miocene
864 Injectite near Santa Cruz, California. In: Hurst, A., Cartwright, J. (Eds.), *Sand*

865 Injectites: Implications for Hydrocarbon Exploration and Production: American
866 Association of Petroleum Geologists, Memoir 87, 151–162.

867 Unruh, J.R., Dumitru, T.A., Sawyer, T.L., 2007. Coupling of early Tertiary extension
868 in the Great Valley forearc basin with blueschist exhumation in the underlying
869 Franciscan accretionary wedge at Mount Diablo, California, GSA Bulletin 119, 1347–
870 1367.

871 Vigorito, M., Hurst, A., Cartwright, J., Scott, A., 2008. Regional-scale shallow crustal
872 remobilization: processes and architecture. Geological Society, London, Special
873 Publications 165, 609-612.

874 Vigorito, M., Hurst, A., 2010. Regional sand injectite architecture as a record of pore
875 pressure evolution and sand redistribution in the shallow crust: insights from the
876 Panoche Giant Injection Complex, California. Journal of Geological Society, London
877 167, 889-904.

878 Yang, Bo, Zhang, Changmin, Li, Shaohua, Du, Jiayuan, Qin, Chenggang, Zhang,
879 Zhongtao, Zhu, Rui, Yu, Ye, 2014. Seismic facies analysis and geological
880 interpretation of large-scale mounds in Pearl River Mouth Basin. Acta Petrolei Sinica
881 35, 37-49.

882

883 **Figure caption**

884

885 **Fig. 1.** Geological map of the study area in California (see inset map for general
886 location): a) Geological map of the western margin of the San Joaquin Valley and

887 associated stratigraphic column (modified from Bartow, 1996); b) Geological map of
888 the Santa Cruz coastal area and associated stratigraphic column (modified from
889 Boehm and Moore, 2002). The stratigraphic position of the giant sand injection
890 complexes cropping out in the study areas is marked. Outcrop locations and places
891 referred to in the text are also shown.

892

893 **Fig. 2.** Simplified structural maps of a) the Panoche/Tumey hills, and b) the Santa
894 Cruz areas showing the preferential SFNF orientations. a) In the Panoche/Tumey
895 hills area, stereoplots (equal-area, lower hemisphere) show preferential NW-SE and
896 WNW-ESE oriented SFNF. b) In the Santa Cruz coastal area, SFNF orientations
897 shown on stereoplots are dominantly NNW-SSE and N-S trending.

898

899 **Fig. 3.** Main types of successions and corresponding fault zone features recognized
900 in the study areas. a) Panoche/Tumey-type successions comprise poorly-
901 consolidated host rock. b) The resulting fault zone generally consists of closed-
902 fracture networks and fine-grained gouge with low permeability. Therefore, faults in
903 Panoche/Tumey-type successions result in a general reduction of the fluid
904 transmissibility. c) Santa Cruz-type successions comprise a well-consolidated host
905 rock. d) Fault zones developed in these successions generally consist of a
906 permeable fracture network surrounding the fault core. Faults in Santa Cruz-type
907 successions generally enhance connectivity and are considered the most efficient
908 pathways for fluid migration. The dashed blue lines indicate the distribution of
909 permeability within the different fault zones.

910

911 **Fig. 4.** Two main types of SFNF recognized in central California. a) Type 1 SFNF
912 related to pressure build-up. b) Type 2a SFNF related to regional extensional
913 tectonics. c) Type 2b SFNF related to regional contractional tectonics. See further
914 explanation in the text.

915

916 **Fig. 5.** Type 1 SFNF from outcrop O1 in the Tumey Gulch area. a), SFNF displaying
917 centimetre-scale offsets and openings of a few centimetres. Note that the different
918 sandstone layers, separated by mudstone horizons, are actually connected with
919 each other through sand filling the SFNF. b) Photograph and c) associated line
920 drawing of conjugate sets of Type 1 SFNF displaying centimetre-scale offsets. Faults
921 die out upwards over tens of centimetres, and the overlying beds remain unaffected
922 by the deformation. Anomalous curvatures of fault planes are related to post-
923 emplacement compaction.

924

925 **Fig. 6.** Type 1 SFNF from outcrop O2 in the Tumey Gulch area. a) Photograph and
926 b) associated line drawing of a SFNF array overlying a remobilized turbidite
927 sandstone body. Fluidisation processes are particularly evident along the irregularly-
928 shaped top surface of the sandstone. SFNF cut just a few metres of overburden
929 while the basal surface remains unaffected by faulting. Note also the anomalous
930 curvature shown by the fault planes due to post-emplacement deformation
931 processes.

932

933 **Fig. 7.** Type 2a SFNF from outcrop O2 in the Tumey Gulch area. a) Photograph and
934 b) associated line drawing of conjugate sets of SFNF showing offsets varying from a
935 few decimetres to metres, and apertures ranging from a few centimetres to some
936 tens of decimetres. Sandstone-filled vertical fractures, consistent with a vertically
937 oriented σ_1 , are also present. Note the SFNF segmentation in the upper part of the
938 outcrop due to post-emplacement compaction. c) Lower hemisphere equal area
939 stereographic projection showing the orientation of the sandstone-filled fault planes
940 (great circles).

941

942 **Fig. 8.** Type 1 SFNF from outcrop O3 in Monocline Ridge. a) Photograph and b)
943 associated line drawing of an array of alternating SFNF and sandstone-filled reverse
944 faults. SFNF show apertures of some centimetres and offsets of few tens of
945 centimetres. Fault 1 displays an almost constant thickness of sand infill while Fault 2
946 shows different lozenge-shaped, en echelon, sandstone-filled segments. Lower
947 hemisphere equal area stereographic projection shows the orientation of the fault
948 planes (great circles).

949

950 **Fig. 9.** Type 2a SFNF from outcrop O4 in the Santa Cruz coastal area. a)
951 Photograph and b) associated line drawing of a SFNF within the Santa Cruz
952 Mudstone. c) Lower hemisphere equal area stereographic projection shows the
953 orientation of the fault planes (great circles).

954

955 **Fig. 10.** Model for the formation of Type 1 SFNF. a) Overpressure in an isolated
956 sandstone layer is built up by the rapid ingress of pore-fluid through a dike
957 connected with deeper overpressured units. Overpressure and the consequent
958 change in shape of the sandstone body causes the failure of the overburden, and the
959 initial injection of fluidized sand along fractures and faults forming a hydrofractured
960 belt. b) These processes evolve with the progressive upward evacuation of sand
961 from the sandstone body and the development of new SFNF. Model for the formation
962 of Type 2 SFNF. c) During the pre-faulting stage, the fluid pressure is equally
963 distributed in the sandstone. d) A fault cutting through the sandstone results in a
964 sudden disturbance in the fluid pressure. The onset of a fluid pressure gradient
965 drives the transfer of fluid from the sandstone toward the low pressured area
966 represented by the fault plane. e) If the fluid reaches the minimum fluidization
967 velocity, the fluidized sand can be carried in suspension and emplaced along the
968 tectonic discontinuity.

969

970 **Fig. 11.** Simplified model of the cross-cutting relationships between Type 1 SFNF
971 and Type 2 SFNF as observed in the PGIC, TGIC and SCIC. a) Emplacement of a
972 sand injection complex. The different architectural elements are organized as
973 proposed by Vigorito et al. (2008). Type 1 SFNF form concomitantly with this event
974 and the age of the faults, as well as that of the entire complex, is obtained by dating
975 the mudstones at the base of the extrudites. b) The emplacement of Type 2 SFNF
976 occurs during a faulting event postdating the emplacement of the main complex. The
977 age of these faults can be determined using standard methods (model is not to
978 scale).

979

980 **Fig. 12.** Type 2a SFNF from outcrop O5 in Tumey Gulch. a) Photograph and b)
981 associated line drawing of SFNF cutting through a pre-existing sandstone intrusion.
982 The host strata consist of diatomaceous mudstones. c) Lower hemisphere equal
983 area stereographic projections showing the orientation of the normal fault planes
984 (great circles and contours). d) Detail of the outcrop O4 showing the intense sand
985 remobilization characterizing the upper margin of the sandstone body, and the
986 fluidized sand intruded along the fault plane. e) Close up showing detail of the fault
987 plane. Note the occurrence of deformation bands and host rock fragments.

988

989 **Fig.13.** Type 2a SFNF from outcrop O4 in Panther Beach. a) Photograph and b)
990 associated line drawing of SFNF cutting through a low-angle dike. Note the thinning
991 of the faulted dike in the vicinity of the fault plane due to the transfer of fluidized sand
992 along the tectonic structure. c) Lower hemisphere equal area stereographic
993 projection showing the orientation of the normal fault plane (great circles).

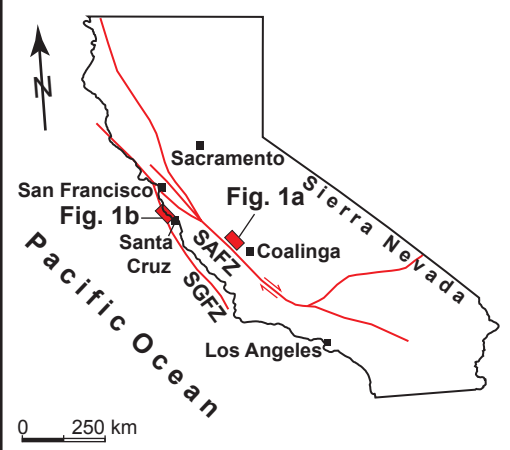
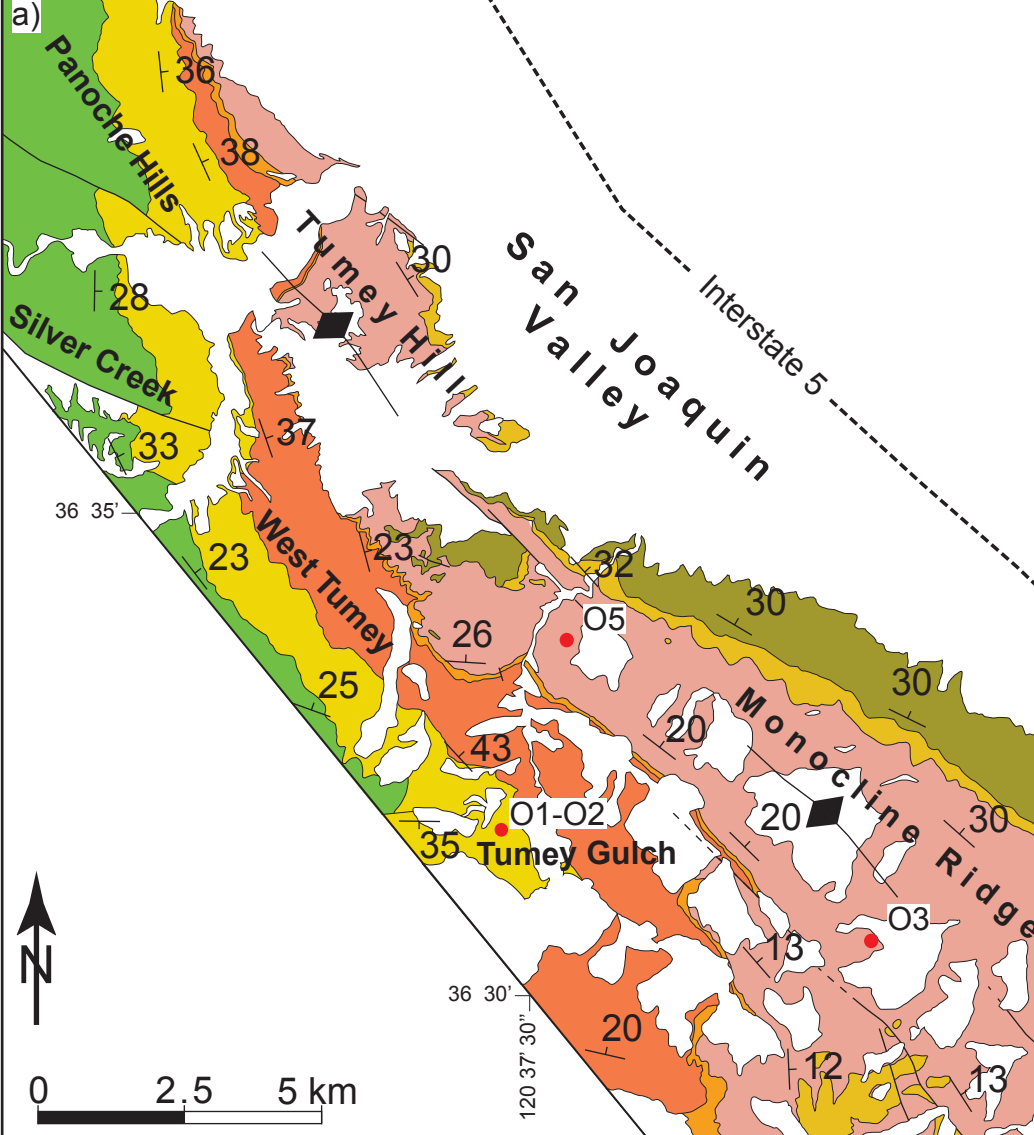
994

995 **Fig. 14.** Impact of SFNF affecting Panoche/Tumey-type succession on reservoir
996 connectivity. a) Ordinary fault cutting through Panoche/Tumey-type successions
997 produces impermeable fine-grained gouge and interrupts the lateral continuity of the
998 sandstone bodies resulting in a barrier to fluid flow transmission. b) The occurrence
999 of sand along the SFNF plane enhances cross- and along fault connectivity. Note
1000 that the offset sandstone layers are still connected after the faulting event. c) Details
1001 of the SFNF plane during sand emplacement. The arrival of fluidized sand is

1002 preceded by water. The impermeable fault gouge along the fault walls is removed by
1003 the turbulent flow.

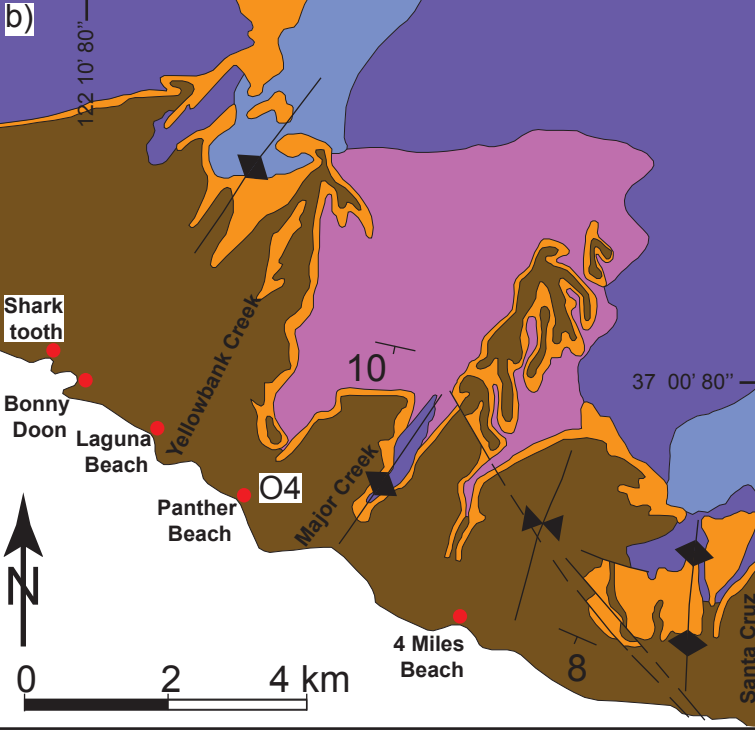
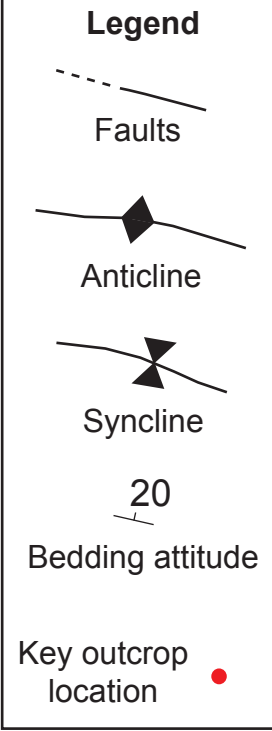
1004

1005 **Fig. 15.** Diagram showing the main characteristics of structurally- and non-
1006 structurally-controlled meso- and large-scale wing-like and conical sandstone
1007 intrusions. a) Stepped and b) conical geometries that are unrelated to regional
1008 tectonics are very common in sand injection complexes. In both cases, sand
1009 emplacement causes jack-up of the overburden that can be recognized at outcrop or
1010 in seismic sections. c), SFNF can produce stepped geometries when a sandstone
1011 body is offset by a fault. However the lateral connectivity between the single steps is
1012 still maintained by the sand contained along the fault plane. d) Conjugate SFNF can
1013 also produce conical-like intrusions connecting the sandstone segments offset by the
1014 fault. In the latter two cases, jack-up of the overburden is not developed. This feature
1015 helps discriminate between structurally- and non-structurally-controlled sandstone
1016 intrusions either at outcrop or in seismic sections.



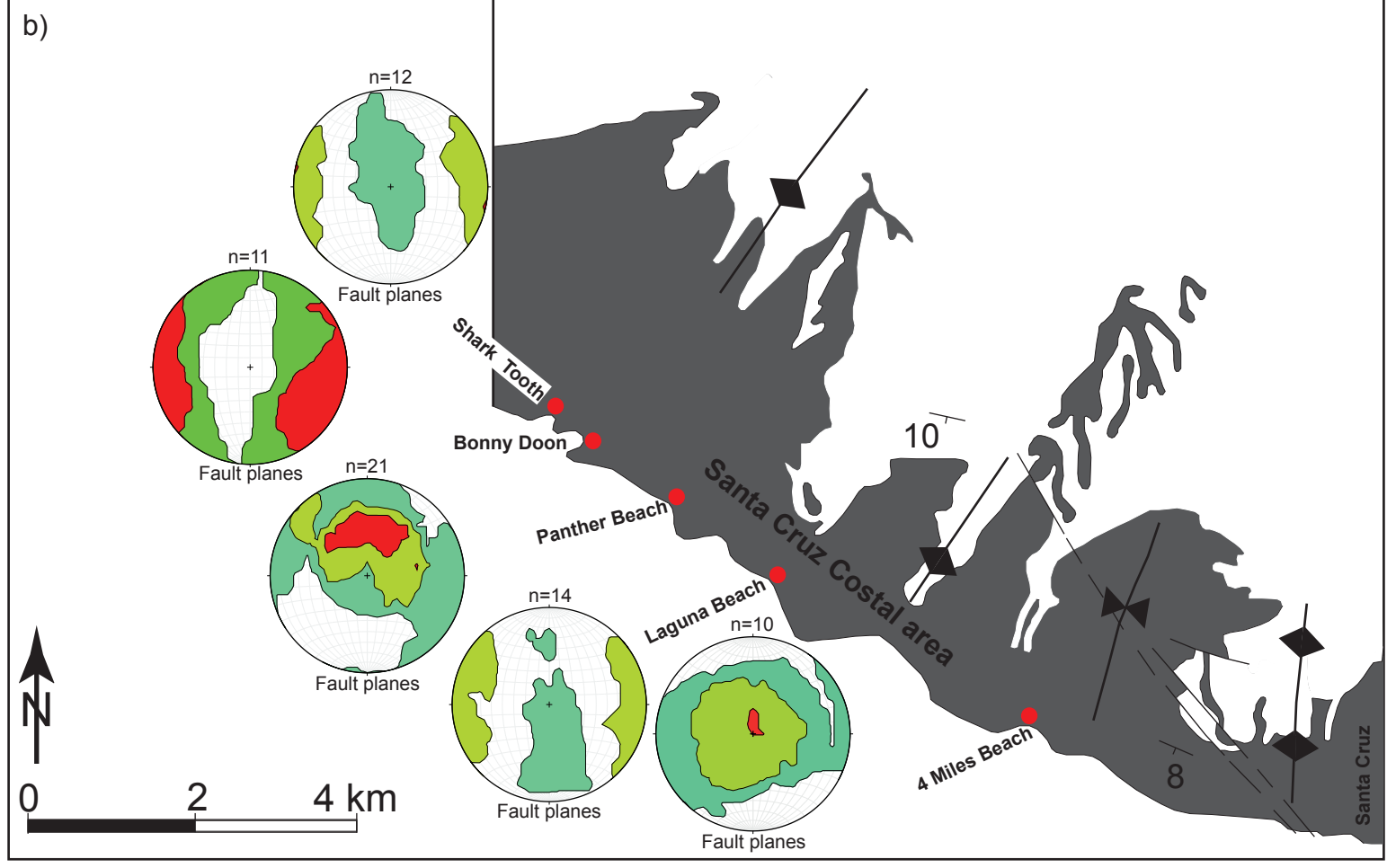
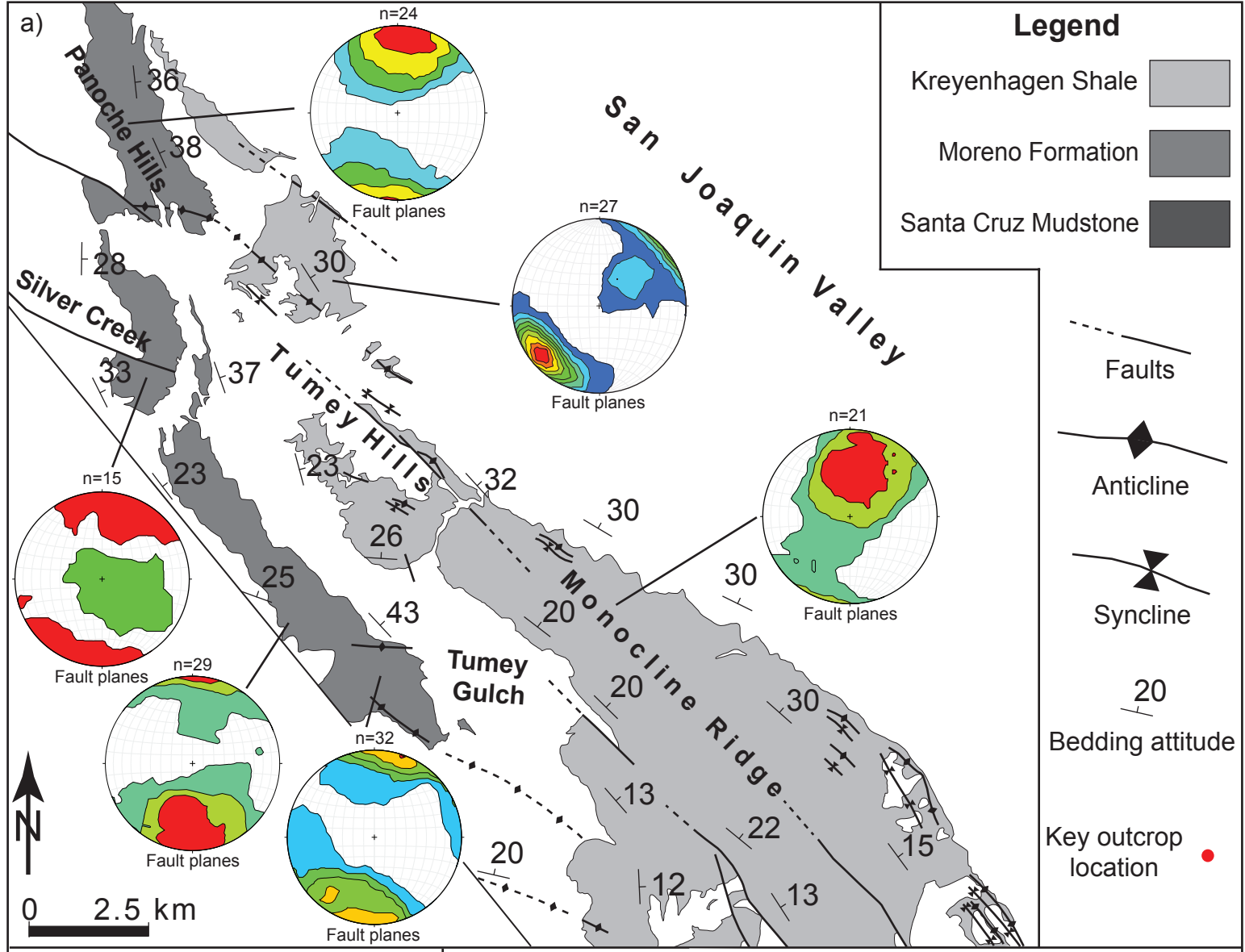
Panoche/Tumey hills area

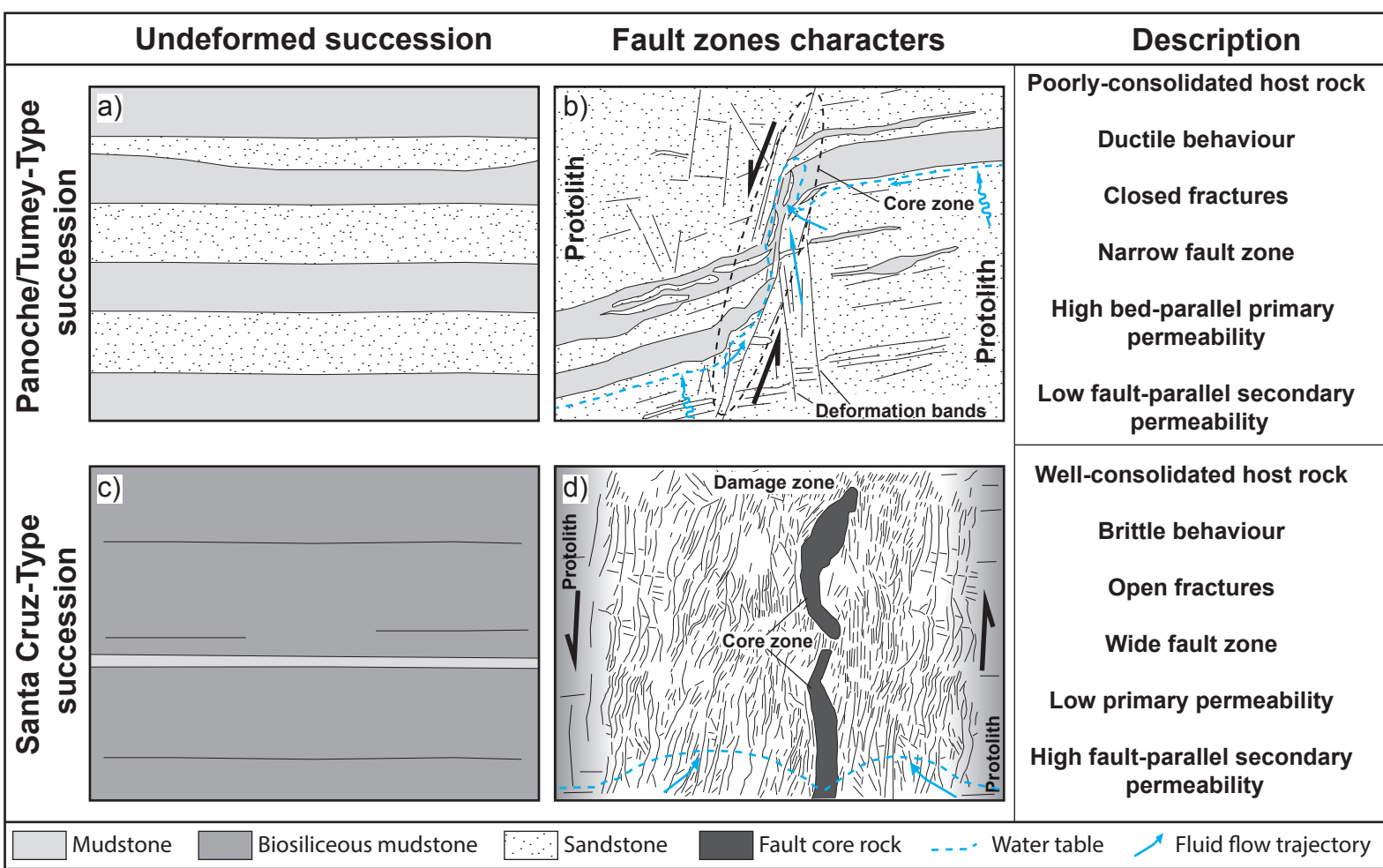
Age	Stratigraphy	Injection Complex
Plei. Ho.	Undifferentiated Quaternary units	
Pli.	Undifferentiated Mio-Pliocene units	
Mioc.		
Olig.	Temblor Fm.	Tumey Giant Injection Complex (TGIC)
Eoc.	Kreyenhagen Shale	
	Domengine Sandstone	
Pal.	Lodo Fm.	
Cretac.	Moreno Fm.	Panoche Giant Injection Complex (PGIC)
	Panoche Fm.	



Santa Cruz area

Age	Stratigraphy	Injection Complex
Upper Miocene to Pliocene	Santa Cruz Mudstone	Santa Cruz Injection Complex (SCIC)
	Santa Margarita Sandstones	
Middle Miocene	Monterrey Formation and Lompico Sandstone undivided	
Paleozoic-Mesozoic	Quartz diorite	
	Metamorphic basement	





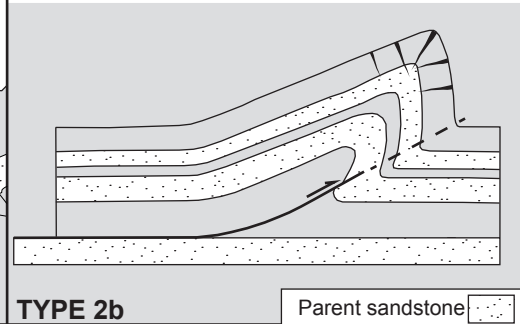
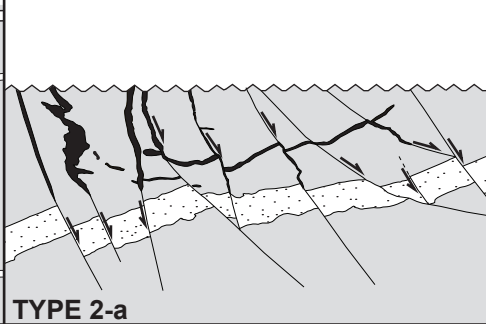
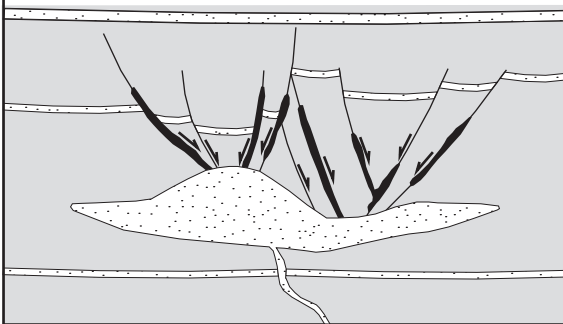
TYPE 1

TYPE 2

a) **Overburden collapse extension**



b) **Regional extensional tectonics**

c) **Outer-arc extension**



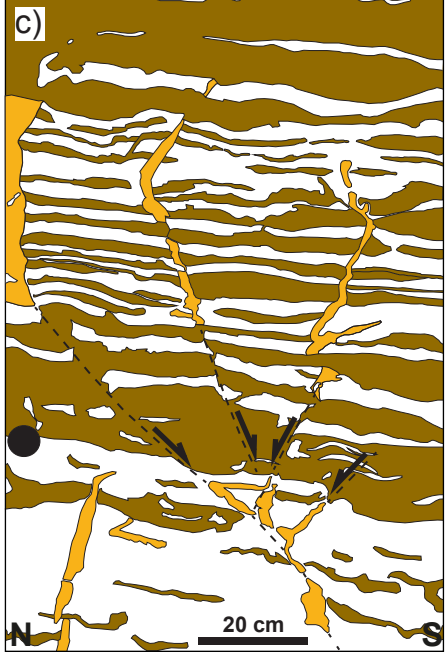
TYPE 2-a

TYPE 2b

Parent sandstone 
Injected sandstone 

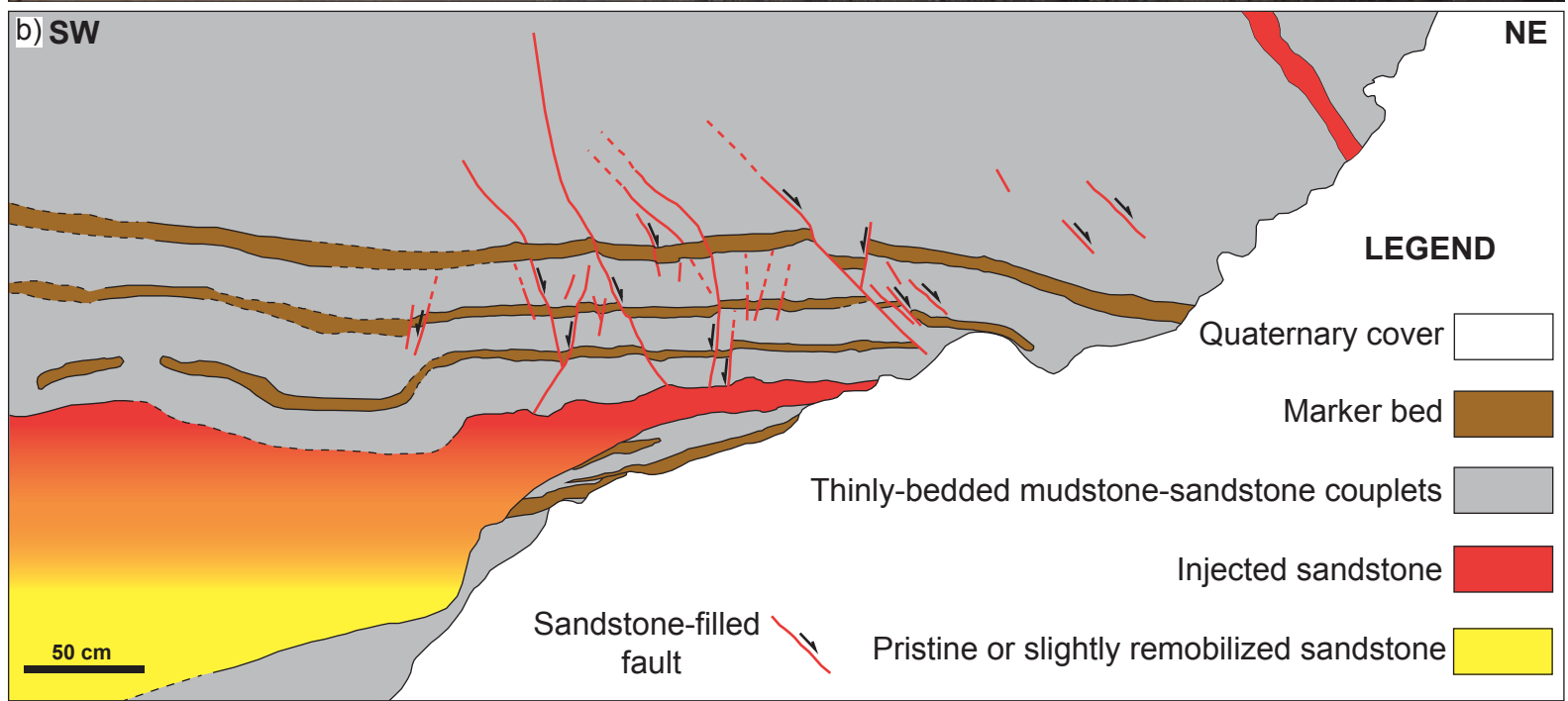
Pressure build up-related faults

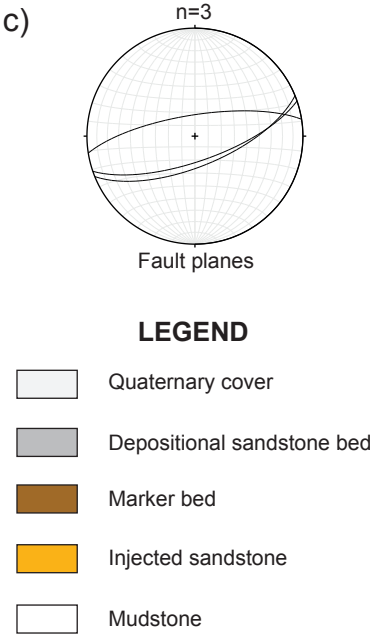
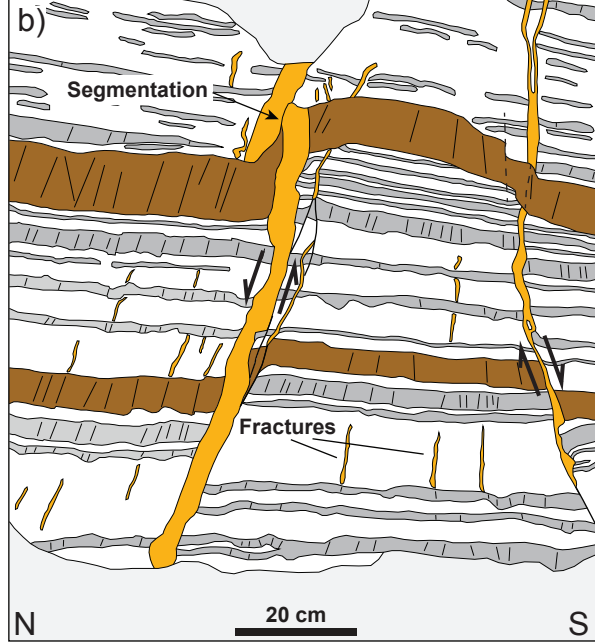
Regional tectonics-related faults

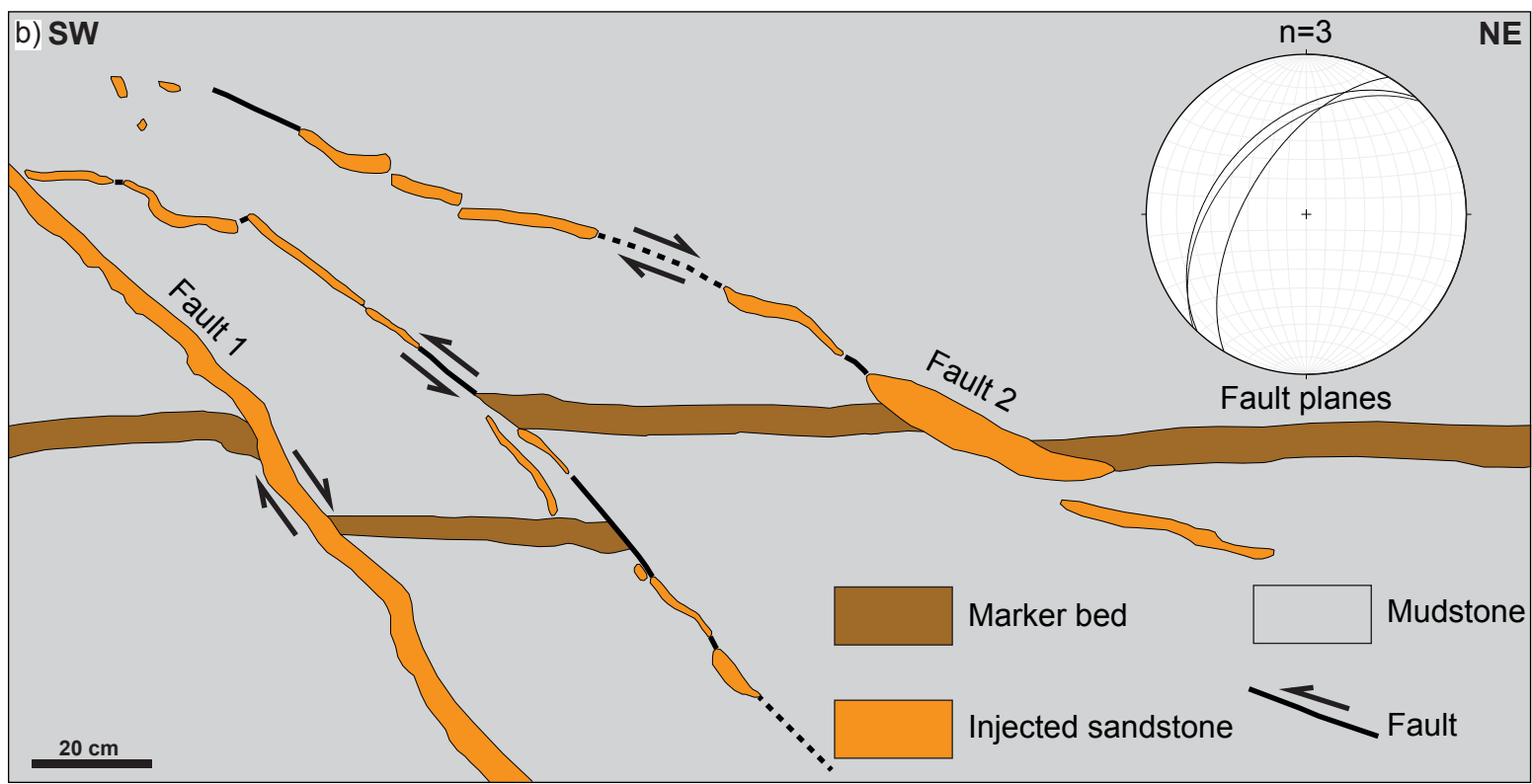


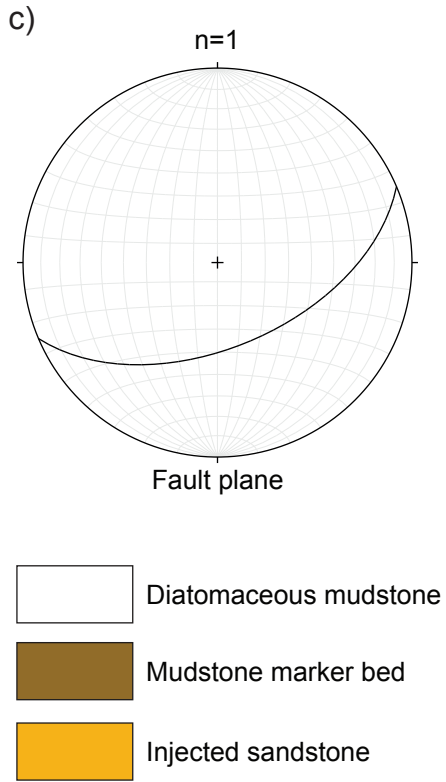
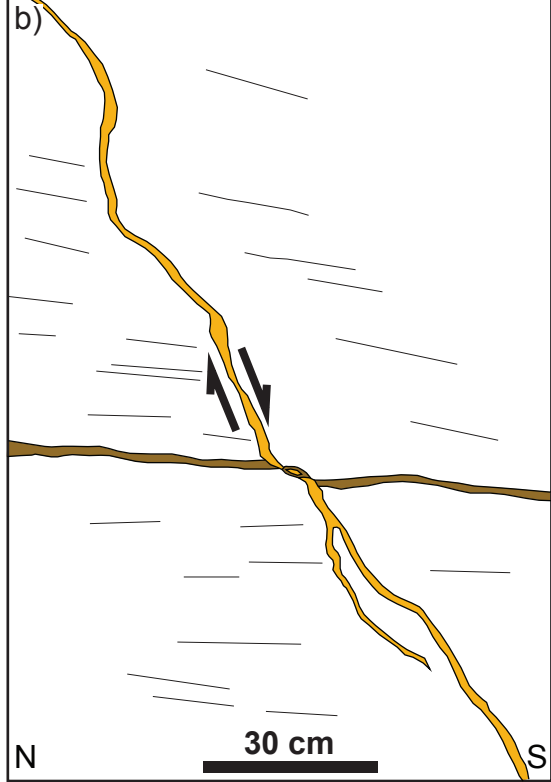
LEGEND

- Depositional Sandstone
- Injected sandstone
- Mudstone
- Fault

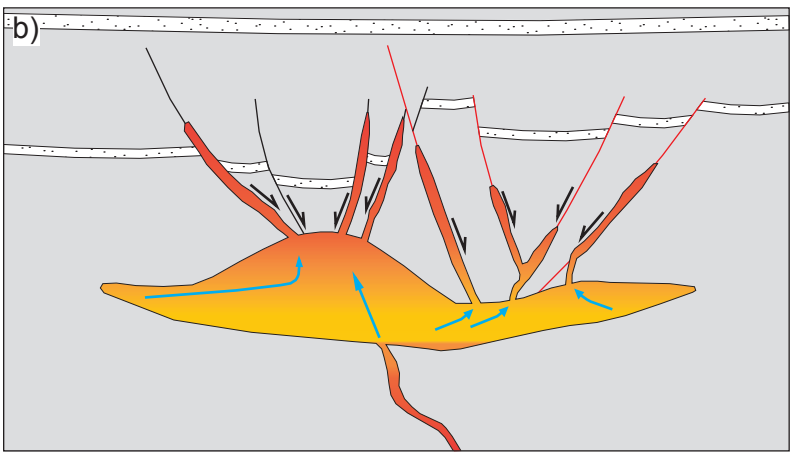
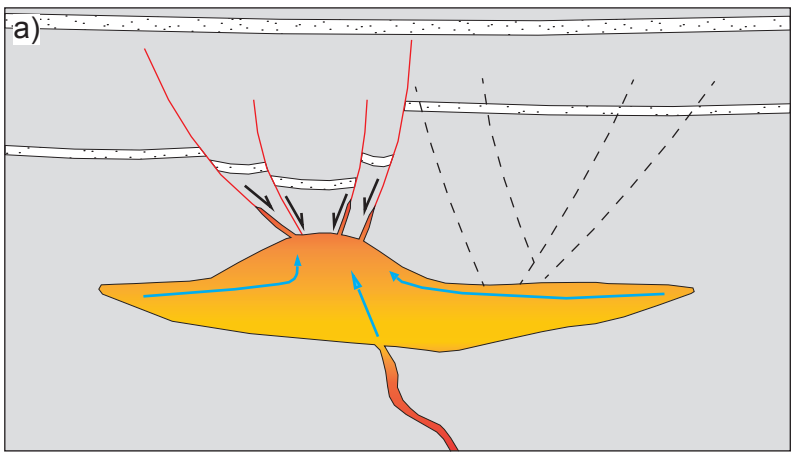




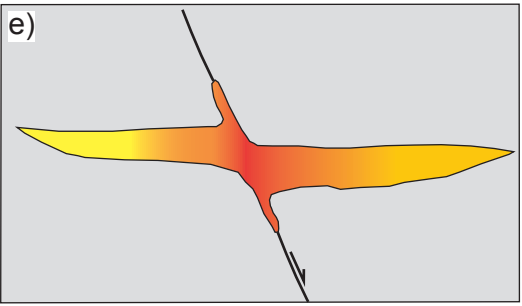
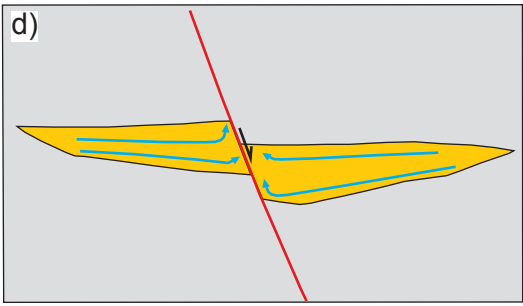
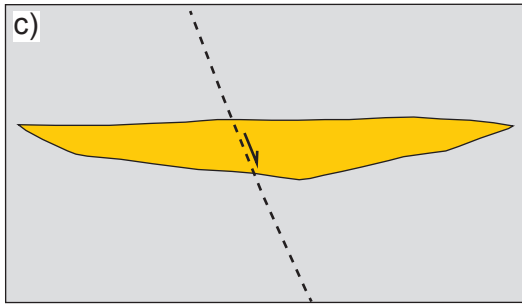





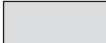
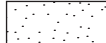
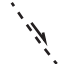




Type 1 SFNF



Type 2 SFNF



	Pristine sandstone		Intensely modified/injected sandstone		Fluid flow trajectory
	Mudstone		Marker bed		Future normal fault
					Active normal fault
					Inactive normal fault

